



ALMA MATER STUDIORUM
UNIVERSITÀ DI BOLOGNA

ARCHIVIO ISTITUZIONALE
DELLA RICERCA

Alma Mater Studiorum Università di Bologna Archivio istituzionale della ricerca

Early life of Neanderthals

This is the final peer-reviewed author's accepted manuscript (postprint) of the following publication:

Published Version:

Nava, A., Lugli, F., Romandini, M., Badino, F., Evans, D., Helbling, A.H., et al. (2020). Early life of Neanderthals. PROCEEDINGS OF THE NATIONAL ACADEMY OF SCIENCES OF THE UNITED STATES OF AMERICA, 117(46), 28719-28726 [10.1073/pnas.2011765117].

Availability:

This version is available at: <https://hdl.handle.net/11585/781091> since: 2020-11-23

Published:

DOI: <http://doi.org/10.1073/pnas.2011765117>

Terms of use:

Some rights reserved. The terms and conditions for the reuse of this version of the manuscript are specified in the publishing policy. For all terms of use and more information see the publisher's website.

This item was downloaded from IRIS Università di Bologna (<https://cris.unibo.it/>).
When citing, please refer to the published version.

(Article begins on next page)

This is the final peer-reviewed accepted manuscript of:

Nava A, Lugli F, Romandini M, Badino F, Evans D, Helbling A, Oxilia G, Arrighi S, Bortolini E, Delpiano D, Duches R, Figus C, Livraghi A, Marciani G, Silvestrini S, Cipriani A, Giovanardi T, Pini R, Nannini N, Tuniz C, Bernardini F, Dori I, Coppa A, Cristiani E, Dean C, Bondioli L, Peresani M, Müller W, Benazzi S (2020) Early life of Neanderthals. *Proceedings of the National Academy of Sciences* 117 (46) 28719-28726.

The final published version is available online at:
<https://doi.org/10.1073/pnas.2011765117>

Rights / License:

The terms and conditions for the reuse of this version of the manuscript are specified in the publishing policy. For all terms of use and more information see the publisher's website.

This item was downloaded from IRIS Università di Bologna (<https://cris.unibo.it/>)

When citing, please refer to the published version.

Main Manuscript for

Early life of Neanderthals

Alessia Nava^{a,b,c,1,2}, Federico Lugli^{d,e,1,2}, Matteo Romandini^{d,f}, Federica Badino^{d,g}, David Evans^{h,i}, Angela H. Helbling^{h,i}, Gregorio Oxilia^d, Simona Arrighi^d, Eugenio Bortolini^d, Davide Delpiano^j, Rossella Duches^k, Carla Figus^d, Alessandra Livraghi^l, Giulia Marciani^d, Sara Silvestrini^d, Anna Cipriani^{e,m}, Tommaso Giovanardi^e, Roberta Pini^g, Claudio Tuniz^{n,o,p}, Federico Bernardini^{n,o}, Irene Dori^{q,r}, Alfredo Coppa^{s,t,u}, Emanuela Cristiani^a, Christopher Dean^{v,w}, Luca Bondioli^{b,x}, Marco Peresani¹, Wolfgang Müller^{h,i,1}, Stefano Benazzi^{d,y,1}

^aDANTE - Diet and ANcient TEchnology Laboratory, Department of Maxillo-Facial Sciences, Sapienza University of Rome, Rome, Italy ^bBioarchaeology Service, Museum of Civilization, Rome, Italy ^cSkeletal Biology Research Centre, School of Anthropology and Conservation, University of Kent, Canterbury, UK ^dDepartment of Cultural Heritage, University of Bologna, Ravenna, Italy ^eDepartment of Chemical and Geological Sciences, University of Modena and Reggio Emilia, Modena, Italy ^fPradis Cave Museum, Clauzetto, Italy ^gInstitute of Environmental Geology and Geoengineering - IGAG CNR ^hInstitute of Geosciences, Goethe University Frankfurt, Frankfurt am Main, Germany ⁱFrankfurt Isotope and Element Research Center (FIERCE), Goethe University Frankfurt, Frankfurt am Main, Germany ^jDepartment of Humanities, University of Ferrara, Italy ^kPrehistory Section - MuSe, Museum of Science, Trento, Italy ^lUniversity Rovira i Virgili, Tarragona, Spain ^mLamont-Doherty Earth Observatory of Columbia University, 61 Route 9W, Palisades NY 10964-1000 USA ⁿAbdus Salam International Centre for Theoretical Physics, Trieste, Italy ^oCentro Fermi, Museo Storico della Fisica e Centro di Studi e Ricerche Enrico Fermi, Roma, Italy ^pCenter for Archaeological Science, University of Wollongong, Wollongong, NSW, Australia ^qSoprintendenza Archeologia, Belle Arti e Paesaggio per le province di Verona, Rovigo e Vicenza, Italy ^rDepartment of Biology, Laboratory of Anthropology, University of Florence, Florence, Italy ^sDepartment of Environmental Biology, Sapienza University of Rome, Rome, Italy ^tDepartment of Genetics, Harvard Medical School, Boston, MA 02115, USA ^uDepartment of Evolutionary Anthropology, University of Vienna, Vienna, Austria ^vDepartment of Earth Sciences, Natural History Museum, London, UK ^wDepartment of Cell and Developmental Biology, University College London, London, UK ^xDepartment of Cultural Heritage, University of Padua, Padua, Italy ^yDepartment of Human Evolution, Max Planck Institute for Evolutionary Anthropology, Leipzig, Germany

¹To whom correspondence may be addressed. Email: alessia.nava@uniroma1.it; federico.lugli6@unibo.it; marco.peresani@unife.it; w.muller@em.uni-frankfurt.de; stefano.benazzi@unibo.it

²These authors contributed equally to this work.

Classification

Biological Sciences, Anthropology

Physical Sciences, Geology

Keywords

Neanderthal ontogeny, nursing strategy, dental histology, spatially-resolved chemical analyses, life histories, Sr/Ca.

Author Contributions

S.B. initiated and led the study; A.N., F.L., M.R., C.D., L.B., M.P., W.M., S.B. designed the study; A.CP., A.H., D.E., F.L., S.S., T.G., W.M. produced chemical/isotopic data; F.BD. and R.P. produced ecological framework; A.N., C.D., L.B. produced histology data; C.T., F.BR. produced the microtomographic record; A.H., A.N., D.E., E.BR., F.L., G.O., L.B., W.M. analyzed or assisted in analysis of data; M.P., M.R., R.D., A.L., D.D. coordinated archaeological excavations; A.CI., C.F., E.BR., E.C., G.M., G.O., I.D., S.A. curated, sampled and/or described analyzed teeth; A.N., C.D., F.L., L.B., S.B., W.M. wrote the manuscript with considerable input from D.E., M.R., F.B., M.P. and with contributions from all authors; all authors contributed to final interpretation of data

This PDF file includes:

Main Text
Figures 1 to 4
Supporting Information

1 Abstract

2 The early onset of weaning in modern humans has been linked to the high nutritional
3 demand of brain development that is intimately connected with infant physiology and
4 growth rate. In Neanderthals, ontogenetic patterns in early life are still debated, with
5 some studies suggesting an accelerated development and others indicating only subtle
6 differences to modern humans. Here we report the onset of weaning and rates of enamel
7 growth using an unprecedented sample set of three late (~70-50 ka) Neanderthals
8 Neanderthals and one Upper Paleolithic modern human from Northeastern-Italy via

9 spatially-resolved chemical/isotopic analyses and histomorphometry of deciduous teeth.
10 Our results reveal that the modern human nursing strategy, with onset of weaning at 5-6
11 months, was already present among these Neanderthals. This evidence, combined with
12 dental development akin to modern humans, highlights their similar metabolic constraints
13 during early life and excludes delayed weaning as a factor contributing to Neanderthals'
14 demise.

15 **Significance Statement**

16 The extent to which Neanderthals differ from us is the current focus of many studies in
17 human evolution. There is debate about their pace of growth and early life metabolic
18 constraints, both of which are still poorly understood. Here we use chemical and isotopic
19 signatures in tandem with enamel growth rates of three Neanderthal milk teeth from
20 Northeastern Italy to explore their early life. Our study shows that these late Neanderthals
21 started to wean children at 5-6 months akin to modern humans, implying similar energy
22 demands during early infancy. Dental growth rates confirm this and follow trajectories
23 comparable with modern humans. Contrary to previous evidence, we suggest that
24 differences in weaning age did not contribute to the demise of Neanderthals.

25

26

27 **Main Text**

28

29 **Introduction**

30

31 Maternal physiology, breastfeeding and the first introduction of supplementary foods are
32 key determinants of human growth (1)(1). The high nutritional demands of the human
33 brain during the first years of life has been identified as the main reason for the early
34 weaning onset in modern humans (2). Indeed, supplementary food is needed when an
35 infant's nutritional requirements exceeds what the mother can provide through breastmilk
36 only (3), an event that in contemporary non-industrial human societies occurs at a modal
37 age of 6 months (4).

38 At present, our knowledge about the link between the pace of child growth, maternal
39 behavior and the onset of weaning among Neanderthals is still scarce. Previous work
40 reported that Neanderthal tooth crowns tend to develop faster than in modern humans,

41 suggesting infant growth was generally accelerated (5). Other earlier work suggested that
42 Neanderthal brain size was comparable to modern humans at birth, but that growth rates
43 in early infancy were higher (6). It has also been shown (7) that Neanderthals followed
44 modes of endocranial development largely similar to modern humans. However, a
45 permanent first molar and a second deciduous molar from La Chaise (France, 127-116 ka
46 and <163 ka respectively) placed rates of Neanderthal tooth growth within the range of
47 modern humans (8). Equally, the association between dental and skeletal growth in a 7-
48 year-old Neanderthal from El Sidròn (Spain, 49 ka) indicated that Neanderthals and
49 modern humans were similar in terms of ontogenetic development, with only small-scale
50 dissimilarities in acceleration or deceleration of skeletal maturation (9). Ba/Ca maps of
51 permanent tooth sections of two early Neanderthals have been interpreted
52 (controversially, see below) as indicators of non-breastmilk food introduction for infants
53 at ~9 (Payre 6, 250 ka) (10) and 7 (Scladina, 120 ka) (11) months of age, later than the
54 modal age in modern humans today. Similarly, wear stage analyses of a large number of
55 deciduous dentitions suggested that introduction of solid food in Neanderthals was
56 delayed by one year compared to modern humans (12).

57 Here we investigate such key aspects of early life in Neanderthals by combining new data
58 on chemical detection of weaning onset with deciduous enamel growth rates. We utilize
59 dental histomorphometry (8, 13), spatially-resolved chemical (14) and isotopic profiles
60 (15, 16) of dental enamel to reconstruct growth rates (13), nursing practices (3) and
61 mobility (15) during the Middle and Upper Paleolithic at high (up to weekly) time
62 resolution. We analyzed an unprecedented set of teeth ($n = 4$) (*SI Appendix*, Text S1)
63 from adjacent archaeological sites in Northeastern Italy (*SI Appendix*, Text S2), dated
64 from the Late Middle to the Early Upper Paleolithic, from Neanderthal-modern human
65 contexts (70-40 ka). These four exfoliated deciduous fossil teeth include three
66 Neanderthals (Fumane 1, a lower left deciduous second molar (17), ~50 ka; Nadale 1, a
67 lower right deciduous first molar (18), ~70 ka; Riparo Broion 1, an upper left deciduous
68 canine (19), ~50 ka) and one Early Upper Paleolithic modern human (UPMH) as
69 comparative specimen from the Fumane site (Fumane 2, an upper right deciduous second
70 incisor (20), Protoaurignacian, ~40 ka) (Fig. 1).

71

72 [Insert Figure 1 here]

73 Exfoliated deciduous teeth derive from individuals who survived permanent tooth
74 replacement and were thus unaffected by any mortality-related bias (23). All teeth come
75 from the same geographic area within a ~55 km radius (Fig. 1), and Fumane 1 and 2 were
76 recovered from different archaeological layers in the same cave, thus allowing direct
77 comparisons in a well-constrained eco-geographical setting.

78 We quantified enamel incremental growth parameters such as postnatal crown formation
79 time and daily enamel secretion rates (24), and we detected the presence of the neonatal
80 line as birth marker (25) by optical light microscopy on thin sections of the deciduous
81 dental crowns. Chemical weaning was investigated via Element/Ca profiles on the same
82 histological sections along the enamel-dentine junction (EDJ) by laser-ablation
83 inductively-coupled-plasma mass spectrometry (LA-ICPMS) (14). In order to detect
84 mobility and/or potential non-local food sources in maternal diet, $^{87}\text{Sr}/^{86}\text{Sr}$ isotope ratio
85 profiles were measured by LA-multi-collector-ICPMS (see Materials and Methods) (15,
86 16).

87 **Results**

88

89 Weaning onset was determined using the topographical variation of the Sr/Ca ratio along
90 the EDJ (14, 26) (*SI Appendix*, Text S3). In exclusively breastfed newborns, the enamel
91 Sr/Ca ratio is markedly lower relative to their prenatal levels (14, 26, 27). This is because
92 human milk is highly enriched in Ca, i.e. Ca is selectively transferred, compared to Sr,
93 across the mammary glands and the placenta (28, 29). Such behavior is confirmed by
94 analyses of breastmilk and infant sera (30). In comparison to human, herbivore milk (and
95 derived formula) is characterized by higher Sr/Ca levels, due to the lower initial trophic
96 position (31). Our dietary model for early life (*SI Appendix*, Text S3) agrees with the
97 expected Sr behavior (14, 27, 32), showing a decrease in Sr/Ca during exclusive
98 breastfeeding and changes in the slope of the profile across the major dietary transitions
99 (i.e. introduction of solid food and end of weaning) (27). This model has been tested
100 successfully in this study on a set of contemporary children's teeth with known dietary
101 histories, including their mothers' eating habits (*SI Appendix*, Text S3 and Fig. S6-S8).
102 Alternative literature models for Ba/Ca (10, 11) point to an increase of Ba/Ca in postnatal
103 enamel during breastfeeding, yet due to even stronger discrimination across biological
104 membranes, Ba/Ca behavior is expected to be similar to Sr/Ca (27), as indeed
105 unequivocally observed here (*SI Appendix*, Text S3 and Fig. S6-S8) and elsewhere (14,
106 33-35).

107 The neonatal lines marking birth were visible in all four archaeological specimens,
108 despite their worn crowns (*SI Appendix*, Fig. S1), allowing the precise estimation of
109 postnatal crown formation times (Fig. 2a). The deciduous first molar Nadale 1 and the
110 deciduous canine Riparo Broion 1 lie within the modern human variability (36-39), while
111 the second deciduous molar Fumane 1 shows a shorter postnatal crown formation time
112 compared with the known archaeological and modern human range (36). The UPMH
113 Fumane 2 deciduous lateral incisor postnatal crown formation time falls instead in the
114 lower limit of the modern human range (37, 39). Overall, the enamel growth rates and the
115 time to form postnatal enamel compares well with modern human data, regardless of
116 differences in their relative tissue volumes and morphologies (5, 8, 9).

117 Daily enamel secretion rates (DSRs) of all specimens, collected in the 100 μm thickness
118 along the enamel dentine junction where laser tracks were run, are reported in Figure 2b,
119 compared with range of variation (min., mean, max.) of modern humans (36-39).
120 Neanderthal DSRs in the first 100 μm of enamel thickness are slower than the
121 corresponding modern human range of variability. However, when the entire dental
122 crown is considered, the distributions of Neanderthal DSRs lie within the lower
123 variability ranges of modern humans (Fig. 2c). The UPMH Fumane 2 DSRs fit the lower
124 portion of the modern human ranges (Fig. 2b,c). The postnatal crown formation times in
125 Neanderthals couple with slower DSRs than in modern humans, as expected given the
126 thinner enamel in Neanderthals' permanent and deciduous teeth (40, 41).

127

128 [Insert Figure 2 here]

129

130 Nadale 1, Fumane 1 & 2 are sufficiently well-preserved from a geochemical point of
131 view, Riparo Broion 1 instead shows some diagenetic overprint (overall Ba is far more
132 affected than Sr; see *SI Appendix*, Text S4 for our diagenesis assessment strategy), but the
133 overall primary elemental signature can still be discerned. Two out of the three
134 Neanderthals, Fumane 1 and Riparo Broion 1, clearly show breastfeeding signals and a
135 decreasing trend in Sr/Ca ratio immediately post-birth, followed by slope changes with
136 the first introduction of non-breastmilk food at 115 days (3.8 months) and 160 days (5.3
137 months; Fig. 3). An even stronger signal of transitional food intake is visible in Fumane 1
138 at 200 days (6.6 months) in the form of a steep increase in Sr/Ca ratio. For the oldest
139 Neanderthal specimen Nadale 1, following a marked variability before birth, the Sr/Ca
140 profile slightly decreases until 140 days (4.7 months). We cannot determine the weaning
141 onset for this individual, who was still being exclusively breastfed by ~5 months of life.
142 The UPMH Fumane 2 has a substantial portion of the prenatal enamel preserved and only
143 a short postnatal enamel growth record (~85 days vs ~55 days respectively). This
144 precludes the chemical detection of the onset of weaning, although the Sr/Ca drop at birth
145 clearly indicates breast-feeding.

146

147 [Insert Figure 3 here]

148

149 The Sr isotope profiles of all investigated teeth show very limited intra-sample
150 variability, confirming that Sr/Ca variations likely relate to changes in dietary end-
151 members rather than diverse geographical provenance of food sources (Fig. 4). These
152 data also give insights in Neanderthal mobility and resource gathering. The $^{87}\text{Sr}/^{86}\text{Sr}$
153 ratios of all Neanderthal teeth overlap with the respective local baselines, defined through
154 archaeological micromammals (42). This suggests that the mothers mostly exploited local
155 food resources. Fumane 1 and Fumane 2, both from the same archaeological site, are
156 characterized by contrasting $^{87}\text{Sr}/^{86}\text{Sr}$ ratios (0.7094 vs 0.7087), indicative of a different
157 use of resources between Neanderthal (local resources) and early UPMH (non-local
158 resources). Such behavior might have been driven by climatic fluctuations, suggesting
159 colder conditions at ~40 ka, dominated by steppe and Alpine meadows (43).

160

161 [Insert Figure 4 here]

162

163 **Discussion**

164

165 Nursing strategies are strictly linked to fertility rates, maternal energetic investment,
166 immune development and infant mortality (44). All of these ultimately contribute to
167 demographic changes of a specific population, with key relevance to the study of human
168 evolution. Prolonged exclusive breastfeeding has a positive impact on an infant's immune
169 system; however, longer breastfeeding negatively influences women's fertility via
170 lactational amenorrhea and thus inter-birth intervals (45). It has been shown that the age
171 peak for weaning onset is reached at around 2.1 times birth weight (46), implying that
172 infants who grow more rapidly need to be weaned earlier than those with a slower pace of
173 growth. Based on modern models, a sustainable timing for infant weaning onset would
174 thus range between 3 and 5 months of age (3). However, contemporary non-industrial

175 societies start weaning their children at a modal age of 6 months (4). Similarly, the World
176 Health Organization recommends exclusive breastfeeding for the first six months of an
177 infant's life (47). This time frame broadly corresponds to the age at which the masticatory
178 apparatus develops, favoring the chewing of first solid foods (3). Such evidence suggests
179 that both skeletal development and infant energy demand contribute to the beginning of
180 the weaning transition. Introduction of non-breastmilk foods is also crucial in reducing
181 the energetic burden of lactation for the mother (4). Breastfeeding represents a substantial
182 investment of energy resources (total caloric content of modern human breastmilk \approx 60
183 kcal/100 mL) (48), entailing an optimal energy allocation between baby feeding and other
184 subsistence-related activities.

185 Our time-resolved chemical data point to an introduction of non-breastmilk foods at \sim 5-6
186 months in the infant diet of two Neanderthals, sooner than previously observed (10, 11)
187 and fully within the modern human pre-industrial figures (4). This evidence, combined
188 with deciduous dental growth akin to modern humans, indicates similar metabolic
189 constraints during early life for the two taxa. The differential food exploitation of Fumane
190 1 and Fumane 2 mothers - who lived in the same site and in a similar environmental
191 setting - suggests a different human-environment interaction between Neanderthals and
192 early UPMHs, as seen in Sr isotope profiles. The Fumane 2 mother spent the end of her
193 pregnancy and the first 55 days after delivery away from the site and was consuming low-
194 biopurified non-local foodstuff with elevated Sr/Ca. Conversely, all Neanderthal mothers
195 spent the last part of their pregnancies and the lactation periods locally and were
196 consuming high-biopurified local food due to the low Sr/Ca-values (see Fig. 3e).

197 The introduction of non-breastmilk food at \sim 5-6 months implies relatively short inter-
198 birth intervals for Neanderthals due to an earlier resumption of post-partum ovulation
199 (49). Moreover, considering the birth weight model (46), we hypothesize that
200 Neanderthal newborns were of similar weight to modern human neonates, pointing to a
201 likely similar gestational history and early-life ontogeny. In a broader context, our results
202 suggest that nursing mode and time among Late Pleistocene humans in Europe were
203 likely not influenced by taxonomic differences in physiology. Therefore, our findings do
204 not support the hypothesis that long postpartum infertility was a contributing factor to the

205 demise of Neanderthals (12). On the other hand, genetic evidence indicates that
206 Neanderthal groups were limited in size (50), which is not in agreement with the shorter
207 inter-birth interval proposed here. Thus, other factors such as e.g. cultural behavior,
208 shorter life-span and high juvenile mortality might have played a focal role in limiting
209 Neanderthal's group size (51, 52).

210

211

212 **Materials and Methods**

213

214 **Thin slices of teeth preparation**

215 Prior to sectioning, a photographic record of the samples was collected. Thin sections of
216 the dental crowns were obtained using the method proposed by others (53, 54) and
217 prepared in the Service of Bioarchaeology of the Museo delle Civiltà in Rome. The
218 sectioning protocol consists of a detailed embedding-cutting-mounting procedure that
219 makes use of dental adhesives, composite resins, and embedding resins. In order to be
220 able to remove the crown from the resin block after sectioning and to restore the dental
221 crowns, the teeth were initially embedded with a reversible resin (Crystalbond 509, SPI
222 Supplies) that does not contaminate chemically the dental tissues and is soluble in
223 Crystalbond cleaning agent (Aramco Products, Inc.). A second embedding in epoxy resin
224 (EpoThin 2, Buehler Ltd) guarantees the stability of the sample during the cutting
225 procedure. The sample was cured for 24 hours at room temperature. Teeth were sectioned
226 using an IsoMet low speed diamond blade microtome (Buehler Ltd). After the first cut, a
227 microscope slide previously treated with liquid silane (3 M RelyX Ceramic Primer) was
228 attached on the exposed surface using a light curing adhesive (3M Scotchbond Multi-
229 Purpose Adhesive) to prevent cracks and any damage during the cutting procedure. A
230 single longitudinal bucco-lingual thin section, averaging 250 μm thick, was cut from each
231 specimen. Each ground section was reduced to a thickness of ~ 150 μm using water
232 resistant abrasive paper of different grits (Carbimet, Buehler Ltd). Finally, the sections
233 were polished with a micro-tissue (Buehler Ltd) and diamond paste with 1 μm size (DB-
234 Suspension, M, Struers).

235 Each thin section was digitally recorded through a camera (Nikon DSFI3) paired with a
236 transmitted light microscope (Olympus BX 60) under polarized light, with different

237 magnifications (40x, 100x, 400x). Overlapping pictures of the dental crown were
238 assembled in a single micrograph using the software ICE 2.0 (Image Composite Editor,
239 Microsoft Research Computational Photography Group) (*SI Appendix*, Fig. S1).

240 After sectioning, the crowns were released from the epoxy block using the Crystalbond
241 cleaning agent and reconstructed using light curing dental restoration resin (Heraeus
242 Charisma Dental Composite Materials).

243 **Sr isotopic analysis by solution MC-ICPMS**

244 To determine local Sr isotope baselines we analyzed archaeological rodent teeth (*SI*
245 *Appendix*, Table S1). Samples were prepared at the Department of Chemical and
246 Geological Sciences of the University of Modena and Reggio Emilia, following protocols
247 described elsewhere (15, 55) and briefly summarized here.

248 From each archaeological site we selected several rodent tooth specimens, according to
249 the stratigraphic distribution of human samples. Enamel from micromammal incisors was
250 manually removed using a scalpel. Few teeth were also analyzed as whole (dentine +
251 enamel). Before the actual digestion with 3M HNO₃, samples (1-5 mg in mass) were
252 washed with MilliQ (ultrasonic bath) and leached with ~0.5 M HNO₃. Sr of the digested
253 specimens was separated from the matrix using 30 µl columns and Triskem Sr-Spec
254 resin.

255 Sr isotope ratios were measured using a Neptune (ThermoFisher) multi-collector
256 inductively-coupled-plasma mass spectrometer (MC-ICPMS) housed at the Centro
257 Interdipartimentale Grandi Strumenti (UNIMORE) during different analytical sessions.
258 Seven Faraday detectors were used to collect signals of the following masses: ⁸²Kr, ⁸³Kr,
259 ⁸⁴Sr, ⁸⁵Rb, ⁸⁶Sr, ⁸⁷Sr, ⁸⁸Sr. Sr solutions were diluted to ~50 ppb and introduced into the
260 Neptune through an APEX desolvating system. Corrections for Kr and Rb interferences
261 follow previous works (15). Mass bias corrections used an exponential law and a ⁸⁸Sr/⁸⁶Sr
262 ratio of 8.375209 (56). The Sr ratios of samples were reported to a SRM987 value of
263 0.710248 (57). During one session, SRM987 yielded an average ⁸⁷Sr/⁸⁶Sr ratio of
264 0.710243 ± 0.000018 (2 S.D., n = 8). Total laboratory Sr blanks did not exceed 100 pg.

265 **Spatially-resolved Sr isotopic analysis by laser-ablation plasma mass spectrometry** 266 **(LA-MC-ICPMS)**

267 LA-MC-ICPMS analyses were conducted at the Frankfurt Isotope and Element Research
268 Center (FIERCE) at Goethe University, Frankfurt am Main (Germany) and closely follow
269 analytical protocols described by Müller & Anczkiewicz (2016) (16); only a brief
270 summary is provided here aiming at highlighting project-specific differences. A 193 nm
271 ArF excimer laser (RESOLUTION S-155, formerly Resonetics, ASI, now Applied Spectra
272 Inc.) equipped with a two-volume LA cell (Laurin Technic) was connected to a
273 NeptunePlus (ThermoFisher) MC-ICPMS using nylon6-tubing and a ‘squid’ signal-
274 smoothing device (58). Ablation took place in a He atmosphere (300 ml/min), with ~1000
275 ml/min Ar added at the funnel of the two-volume LA cell and 3.5 ml/min N₂ before the
276 squid. Laser fluence on target was ~5 J/cm².

277 Spatially-resolved Sr isotopic analyses of dental enamel were performed on the thin
278 sections (100-150 µm thick) used for enamel histology and trace element analysis (see
279 below), in continuous profiling mode following the enamel-dentine-junction (EDJ) from
280 apex to cervix (14), less than 100 µm away from the EDJ. Tuning of the LA-MC-ICPMS
281 used NIST 616 glass for best sensitivity (⁸⁸Sr) while maintaining robust plasma
282 conditions, i.e. ²³²Th¹⁶O/²³²Th <0.5% and ²³²Th/²³⁸U >0.95 with RF-power of ~1360 W.
283 In view of the low Sr concentrations in these human enamel samples (~60-100 µg/g), we
284 utilized 130 µm spots, a scan speed of 5 µm/s and a repetition rate of 20 Hz to maintain
285 ⁸⁸Sr ion currents of ~2-3.5 x 10⁻¹¹ A. Nine Faraday detectors were used to collect the ion
286 currents of the following masses (m/z): ⁸³Kr, ~83.5, ⁸⁴Sr, ⁸⁵Rb, ⁸⁶Sr, ~86.5, ⁸⁷Sr, ⁸⁸Sr,
287 ⁹⁰Zr. Baseline, interference and mass bias corrections follow (16). The isotopically-
288 homogenous (Sr) enameloid of a modern shark was used to assess accuracy of the Sr-
289 isotopic analysis and yielded ⁸⁷Sr/⁸⁶Sr = 0.70916 ± 2 and ⁸⁴Sr/⁸⁶Sr = 0.0565 ± 1 (2 S.D.).
290 Raw data are reported in Dataset S1.

291 **Spatially-resolved elemental ratio and concentration analysis by laser-ablation** 292 **plasma mass spectrometry (LA- ICPMS)**

293 All LA-ICPMS analyses of archaeological samples were conducted at the Frankfurt
294 Isotope and Element Research Center (FIERCE) at Goethe University, Frankfurt am
295 Main (Germany), using the same LA system described above, but connected via a squid
296 smoothing-device to an Element XR ICPMS. Analytical protocols follow those by Müller

297 et al (2019) (14); and only a brief summary is provided here aimed at highlighting
298 differences. LA-ICPMS trace element ratios/concentrations of the comparative
299 contemporary teeth were obtained at Royal Holloway University of London (RHUL)
300 using the RESOLution M-50 prototype LA system featuring a Laurin two-volume LA cell
301 (58), coupled to an Agilent 8900 triple-quadrupole-ICPMS (ICP-QQQ or ICP-MS/MS).
302 Compositional profiles were analyzed parallel and as close as possible to the EDJ,
303 following the same tracks used for Sr isotope analyses. We employed 15 μm spot sizes
304 (FIERCE) or 6 μm (MCS3, RHUL) and 34 μm (MCS1 and 2, RHUL), respectively, as
305 well as a scan speed of 5 $\mu\text{m}/\text{s}$ and a repetition rate of 15 Hz; prior to acquisition, samples
306 were pre-cleaned using slightly larger spot sizes (22 - 57 μm), 20 Hz and faster scan
307 speeds (25 - 50 $\mu\text{m}/\text{s}$); laser fluence was $\sim 5 \text{ J}/\text{cm}^2$. The following isotopes (m/z) were
308 analyzed: ^{25}Mg , ^{27}Al , ^{43}Ca , (^{44}Ca), ^{55}Mn , ^{66}Zn , ^{85}Rb , (^{86}Sr), ^{88}Sr , ^{89}Y , ^{138}Ba , ^{140}Ce , (^{166}Er ,
309 ^{172}Yb), ^{208}Pb , ^{238}U . The total sweep times for the Element XR and the 8900 ICP-MS/MS
310 were ~ 0.8 and 0.4-0.5 s, respectively; however, because of the slow scan speeds, this
311 small difference has no effect on the compositional profiles presented here. Primary
312 standardization was achieved using NIST SRM612. Ca was employed as internal
313 standard (^{43}Ca); [Ca] at 37 %m/m was used to calculate concentrations for unknown
314 bioapatites, although not required for X/Ca ratios. Accuracy and reproducibility were
315 assessed using repeated analyses of the STDP-X-glasses (59) as secondary reference
316 materials; the respective values for Sr/Ca and Ba/Ca (the element/Ca ratios of principal
317 interest) here are $1.8 \pm 6.6\%$ and $-0.2 \pm 6.0\%$ (%bias ± 2 S.D. (%)); this compares well
318 with the long-term reproducibility for these analytes reported previously (60). Raw data
319 are reported in Dataset S2 and S3.

320 The compositional/isotopic profiles were smoothed with a locally weighted polynomial
321 regression fit (LOWESS), with its associated standard error range (± 3 S.E.) for each
322 predicted value (61). The statistical package R (ver. 3.6.2) (62) was used for all statistical
323 computations and generation of graphs.

324 **Assessment of the enamel growth parameters and of the chronologies along the laser**
325 **tracks**

326 Dental enamel is capable of recording, at microscopic level during its formation, regular
327 physiological and rhythmic growth markers (63-65). These incremental markings are
328 visible under transmitted light in longitudinal histological thin sections of dental crowns.
329 Enamel forms in a rhythmic manner, reflecting the regular incremental secretion of the
330 matrix by the ameloblasts (i.e. the enamel forming cells). The rhythmical growth of
331 enamel is expressed in humans at two different levels: a circadian rhythm that produces
332 the daily cross striations (66, 67) and a longer period rhythmic marking (near- weekly in
333 humans) that give rise to the Retzius lines (68). Physiological stresses affecting the
334 individual during tooth growth cause a disruption of the enamel matrix secretion and
335 mark the corresponding position of the secretory ameloblast front, producing Accentuated
336 (Retzius) Lines (ALs) (69, 70). The birth event is recorded in the forming enamel of
337 individuals surviving the perinatal stage, and leaves - usually the first - Accentuated Line,
338 namely the Neonatal Line (NL) (25, 71, 72).

339 The time taken to form the dental crown after birth was measured on each thin section
340 adapting the methods described in literature (39, 73).

341 A prism segment starting from the most apical available point on the enamel dentine
342 junction (EDJ) and extending from this point to an isochronous incremental line (i.e. the
343 NL, an AL or a Retzius line) was measured. The incremental line was followed back to
344 the EDJ and a second prism segment was measured in the same way. The process was
345 repeated until the most cervical enamel was reached. The crown formation time is equal
346 to the sum of the single prism segments. To obtain time (in days) from the prism length
347 measurements, local daily secretion rates (24) (DSR) were calculated around the prism
348 segments and within 100 μm from the EDJ, by counting visible consecutive cross
349 striations and dividing it by the corresponding prism length. The chronologies of
350 accentuated lines (ALs) in the modern sample closely match the timing of known
351 disruptive life history events in the mother (illness, surgery) and infant, and so are well
352 within the range or error (1.2-4.4%) observed for this histological ageing method (63).

353 DSRs were collected across the whole crown on spots chosen randomly in order to get
354 the DSRs distribution. Groups of cross striations ranging from 3 to 7 were measured. For
355 each crown the number of measured spots ranges between 49 and 233.

356 After LA-ICPMS analyses, a micrograph highlighting the laser tracks was acquired at
357 50x magnification. This was superimposed to a second micrograph of the same thin
358 section at 100x magnification, to gain better visibility of the enamel microstructural
359 features. The chronologies along the laser tracks were obtained matching the tracks with
360 the isochronous lines.

361
362
363

Acknowledgments

364 Archaeological excavations at Fumane and De Nadale are coordinated by University of
365 Ferrara and supported by public institutions (Fumane: Lessinia Mountain Community,
366 Fumane Municipality, BIMAdige; De Nadale: Zovencedo Municipality) and private
367 associations and companies (De Nadale: RAASM). Archaeological excavations at Riparo
368 Broion are coordinated by University of Bologna and University of Ferrara and supported
369 by H2020 grant 724046 – SUCCESS. Superintendency SAPAB-VR provided access to
370 the samples of Nadale 1, Riparo Broion 1, Fumane 1 and Fumane 2. We thank the parents
371 and the children who donated deciduous teeth and who carefully recorded the dietary
372 events of their children. Michael P. Richards and Marcello Mannino are thanked for
373 stimulating discussions and for having initiated isotopic studies of the specimens at
374 Fumane. This project was funded by the European Research Council (ERC) under the
375 European Union’s Horizon 2020 Research and Innovation Programme (grant agreement
376 No 724046 – SUCCESS awarded to Stefano Benazzi – erc-success.eu and grant
377 agreement No 639286 – HIDDEN FOODS awarded to Emanuela Cristiani –
378 www.hiddenfoods.org). FIERCE is financially supported by the Wilhelm and Else
379 Heraeus Foundation and by the Deutsche Forschungsgemeinschaft (DFG, INST 161/921-
380 1 FUGG and INST 161/923-1 FUGG), which is gratefully acknowledged. LA-ICPMS
381 analyses at Royal Holloway University of London, used for early comparative samples
382 shown in the supporting material, was supported by NERC equipment funding (NERC
383 CC073).

384
385
386
387
388
389

390 **References**

391
392

- 393 1. Sellen DW (2007) Evolution of infant and young child feeding: implications for
394 contemporary public health. *Annu. Rev. Nutr.* 27:123-148.
- 395 2. Kennedy GE (2005) From the ape's dilemma to the weanling's dilemma: early
396 weaning and its evolutionary context. *Journal of human evolution* 48(2):123-145.
- 397 3. Humphrey LT (2010) Weaning behaviour in human evolution. *Seminars in Cell*
398 *and Developmental Biology* 21(4):453-461.
- 399 4. Sellen DW (2001) Comparison of infant feeding patterns reported for
400 nonindustrial populations with current recommendations. *The Journal of nutrition*
401 131(10):2707-2715.
- 402 5. Smith TM, *et al.* (2010) Dental evidence for ontogenetic differences between
403 modern humans and Neanderthals. *Proceedings of the National Academy of*
404 *Sciences of the United States of America* 107(49):20923-20928.
- 405 6. Gunz P, Neubauer S, Maureille B, & Hublin J-J (2010) Brain development after
406 birth differs between Neanderthals and modern humans. *Current biology*
407 20(21):R921-R922.
- 408 7. de León MSP, Bienvenu T, Akazawa T, & Zollikofer CP (2016) Brain
409 development is similar in Neanderthals and modern humans. *Current Biology*
410 26(14):R665-R666.
- 411 8. Macchiarelli R, *et al.* (2006) How Neanderthal molar teeth grew. *Nature*
412 444(7120):748.
- 413 9. Rosas A, *et al.* (2017) The growth pattern of Neandertals, reconstructed from a
414 juvenile skeleton from El Sidrón (Spain). *Science* 357(6357):1282-1287.
- 415 10. Smith TM, *et al.* (2018) Wintertime stress, nursing, and lead exposure in
416 Neanderthal children. *Science Advances* 4(10):eaau9483.
- 417 11. Austin C, *et al.* (2013) Barium distributions in teeth reveal early-life dietary
418 transitions in primates. *Nature* 498(7453):216-219.
- 419 12. Skinner M (1997) Dental wear in immature Late Pleistocene European hominines.
420 *J. Archaeol. Sci.* 24(8):677-700.
- 421 13. Dean MC (2010) Retrieving chronological age from dental remains of early fossil
422 hominins to reconstruct human growth in the past. *Philosophical Transactions of*
423 *the Royal Society of London B: Biological Sciences* 365(1556):3397-3410.
- 424 14. Müller W, *et al.* (2019) Enamel mineralization and compositional time-resolution
425 in human teeth evaluated via histologically-defined LA-ICPMS profiles.
426 *Geochimica et Cosmochimica Acta* 255:105-126.
- 427 15. Lugli F, *et al.* (2019) Strontium and stable isotope evidence of human mobility
428 strategies across the Last Glacial Maximum in southern Italy. *Nature ecology &*
429 *evolution* 3(6):905-911.
- 430 16. Müller W & Anczkiewicz R (2016) Accuracy of laser-ablation (LA)-MC-ICPMS
431 Sr isotope analysis of (bio) apatite—a problem reassessed. *Journal of Analytical*
432 *Atomic Spectrometry* 31(1):259-269.
- 433 17. Benazzi S, *et al.* (2014) Middle Paleolithic and Uluzzian human remains from
434 Fumane Cave, Italy. *Journal of Human Evolution* 70:61-68.

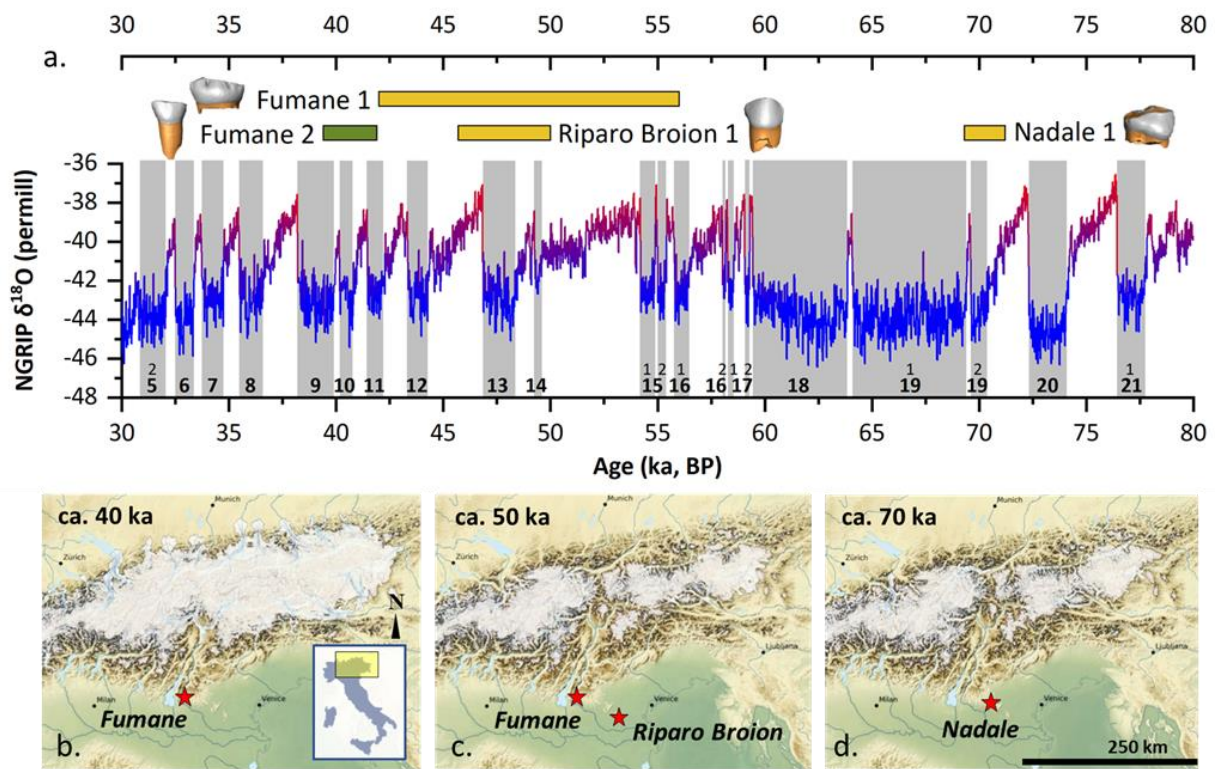
- 435 18. Arnaud J, *et al.* (2017) A Neanderthal deciduous human molar with incipient
436 carious infection from the Middle Palaeolithic De Nadale cave, Italy. *American*
437 *journal of physical anthropology* 162(2):370-376.
- 438 19. Romandini M, *et al.* (in review) A late Neanderthal tooth from northeastern Italy.
439 *Journal of Human Evolution*.
- 440 20. Benazzi S, *et al.* (2015) The makers of the Protoaurignacian and implications for
441 Neandertal extinction. *Science* 348(6236):793-796.
- 442 21. Rasmussen SO, *et al.* (2014) A stratigraphic framework for abrupt climatic
443 changes during the Last Glacial period based on three synchronized Greenland
444 ice-core records: refining and extending the INTIMATE event stratigraphy.
445 *Quaternary Science Reviews* 106:14-28.
- 446 22. Seguinot J, *et al.* (2018) Modelling last glacial cycle ice dynamics in the Alps.
447 *The Cryosphere* 12(10):3265-3285.
- 448 23. Wood JW, *et al.* (1992) The osteological paradox: problems of inferring
449 prehistoric health from skeletal samples [and comments and reply]. *Current*
450 *Anthropology* 33(4):343-370.
- 451 24. Nava A, *et al.* (2017) New Regression Formula to Estimate the Prenatal Crown
452 Formation Time of Human Deciduous Central Incisors Derived from a Roman
453 Imperial Sample (Velia, Salerno, I-II cent. CE). *PloS ONE* 12(7):e0180104.
- 454 25. Dean MC, Spiers KM, Garrovoet J, & Le Cabec A (2019) Synchrotron X-ray
455 fluorescence mapping of Ca, Sr and Zn at the neonatal line in human deciduous
456 teeth reflects changing perinatal physiology. *Archives of oral biology* 104:90-102.
- 457 26. Humphrey LT, Dean MC, Jeffries TE, & Penn M (2008) Unlocking evidence of
458 early diet from tooth enamel. *Proceedings of the National Academy of Sciences of*
459 *the United States of America* 105(19):6834-6839.
- 460 27. Humphrey LT (2014) Isotopic and trace element evidence of dietary transitions in
461 early life. *Annals of Human Biology* 41(4):348-357.
- 462 28. Humphrey LT, Dirks W, Dean MC, & Jeffries TE (2008) Tracking dietary
463 transitions in weanling baboons (*Papio hamadryas anubis*) using
464 strontium/calcium ratios in enamel. *Folia Primatologica* 79(4):197-212.
- 465 29. Rossipal E, Krachler M, Li F, & Micetic-Turk D (2000) Investigation of the
466 transport of trace elements across barriers in humans: studies of placental and
467 mammary transfer. *Acta Paediatrica* 89(10):1190-1195.
- 468 30. Krachler M, Rossipal E, & Micetic-Turk D (1999) Concentrations of trace
469 elements in sera of newborns, young infants, and adults. *Biological trace element*
470 *research* 68(2):121.
- 471 31. Burton JH, Price TD, & Middleton WD (1999) Correlation of bone Ba/Ca and
472 Sr/Ca due to biological purification of calcium. *J. Archaeol. Sci.* 26(6):609-616.
- 473 32. Tsutaya T & Yoneda M (2015) Reconstruction of breastfeeding and weaning
474 practices using stable isotope and trace element analyses: a review. *American*
475 *Journal of Physical Anthropology* 156(S59):2-21.
- 476 33. Peek S & Clementz MT (2012) Sr/Ca and Ba/Ca variations in environmental and
477 biological sources: a survey of marine and terrestrial systems. *Geochimica et*
478 *Cosmochimica Acta* 95:36-52.

- 479 34. Metcalfe JZ, Longstaffe FJ, & Zazula GD (2010) Nursing, weaning, and tooth
480 development in woolly mammoths from Old Crow, Yukon, Canada: implications
481 for Pleistocene extinctions. *Palaeogeography, Palaeoclimatology, Palaeoecology*
482 298(3-4):257-270.
- 483 35. Tacail T, Kovačiková L, Brůžek J, & Balter V (2017) Spatial distribution of trace
484 element Ca-normalized ratios in primary and permanent human tooth enamel.
485 *Science of the Total Environment* 603:308-318.
- 486 36. Mahoney P (2011) Human deciduous mandibular molar incremental enamel
487 development. *American Journal of Physical Anthropology* 144(2):204-214.
- 488 37. Mahoney P (2012) Incremental enamel development in modern human deciduous
489 anterior teeth. *American Journal of Physical Anthropology* 147(4):637-651.
- 490 38. Dean MC, Humphrey L, Groom A, & Hassett B (2020) Variation in the timing of
491 enamel formation in modern human deciduous canines. *Archives of Oral*
492 *Biology*:104719.
- 493 39. Birch W & Dean MC (2014) A method of calculating human deciduous crown
494 formation times and of estimating the chronological ages of stressful events
495 occurring during deciduous enamel formation. *Journal of Forensic and Legal*
496 *Medicine* 22:127-144.
- 497 40. Fornai C, *et al.* (2014) Enamel thickness variation of deciduous first and second
498 upper molars in modern humans and Neanderthals. *Journal of human evolution*
499 76:83-91.
- 500 41. Olejniczak AJ, *et al.* (2008) Dental tissue proportions and enamel thickness in
501 Neandertal and modern human molars. *Journal of Human Evolution* 55(1):12-23.
- 502 42. López-García JM, Berto C, & Peresani M (2019) Environmental and climatic
503 context of the hominin occurrence in northeastern Italy from the late Middle to
504 Late Pleistocene inferred from small-mammal assemblages. *Quaternary Science*
505 *Reviews* 216:18-33.
- 506 43. López-García JM, dalla Valle C, Cremaschi M, & Peresani M (2015)
507 Reconstruction of the Neanderthal and Modern Human landscape and climate
508 from the Fumane cave sequence (Verona, Italy) using small-mammal
509 assemblages. *Quaternary Science Reviews* 128:1-13.
- 510 44. Miller EM (2018) Beyond passive immunity: Breastfeeding, milk and
511 collaborative mother-infant immune systems. *Breastfeeding: New*
512 *Anthropological Approaches*, (Routledge, New York), pp 26-39.
- 513 45. Campbell KL & Wood JW (1988) Fertility in traditional societies. *Natural human*
514 *fertility*, (Springer), pp 39-69.
- 515 46. Lee PC (1996) The meanings of weaning: growth, lactation, and life history.
516 *Evolutionary Anthropology: Issues, News, and Reviews: Issues, News, and*
517 *Reviews* 5(3):87-98.
- 518 47. World Health Organization (2009) Infant and young child feeding: model chapter
519 for textbooks for medical students and allied health professionals.
- 520 48. Prentice P, *et al.* (2016) Breast milk nutrient content and infancy growth. *Acta*
521 *Paediatrica* 105(6):641-647.

- 522 49. Taylor HW, Vázquez-Geffroy M, Samuels SJ, & Taylor DM (1999) Continuously
523 recorded suckling behaviour and its effect on lactational amenorrhoea. *Journal of*
524 *biosocial science* 31(3):289-310.
- 525 50. Prüfer K, *et al.* (2014) The complete genome sequence of a Neanderthal from the
526 Altai Mountains. *Nature* 505(7481):43-49.
- 527 51. Garber CM (1947) Eskimo infanticide. *The Scientific Monthly* 64(2):98-102.
- 528 52. Trinkaus E (1995) Neanderthal mortality patterns. *J. Archaeol. Sci.* 22(1):121-
529 142.
- 530 53. Nava A (2018) Hominin dental enamel: an integrated approach to the study of
531 formation, maturation, and morphology (Unpublished doctoral dissertation). PhD
532 (Sapienza University of Rome, Rome).
- 533 54. Caropreso S, *et al.* (2000) Thin sections for hard tissue histology: a new
534 procedure. *Journal of Microscopy* 199(3):244-247.
- 535 55. Weber M, Lugli F, Jochum KP, Cipriani A, & Scholz D (2018) Calcium
536 carbonate and phosphate reference materials for monitoring bulk and
537 microanalytical determination of Sr isotopes. *Geostandards and Geoanalytical*
538 *Research* 42(1):77-89.
- 539 56. Steiger RH & Jäger E (1977) Subcommittee on geochronology: convention on
540 the use of decay constants in geo-and cosmochronology. *Earth and planetary*
541 *science letters* 36(3):359-362.
- 542 57. McArthur JM, Howarth R, & Bailey T (2001) Strontium isotope stratigraphy:
543 LOWESS version 3: best fit to the marine Sr-isotope curve for 0–509 Ma and
544 accompanying look-up table for deriving numerical age. *The Journal of Geology*
545 109(2):155-170.
- 546 58. Müller W, Shelley M, Miller P, & Broude S (2009) Initial performance metrics of
547 a new custom-designed ArF excimer LA-ICPMS system coupled to a two-volume
548 laser-ablation cell. *Journal of Analytical Atomic Spectrometry* 24:209-214.
- 549 59. Klemme S, *et al.* (2008) Synthesis and preliminary characterisation of new
550 silicate, phosphate and titanite reference glasses. *Geostandards and Geoanalytical*
551 *Research* 32(1):39-54.
- 552 60. Evans D & Müller W (2018) Automated extraction of a five-year LA-ICP-MS
553 trace element data set of ten common glass and carbonate reference materials:
554 Long-term data quality, optimisation and laser cell homogeneity. *Geostandards*
555 *and Geoanalytical Research* 42(2):159-188.
- 556 61. Cleveland WS, Grosse E, & Shyu WM (1992) Local regression models.
557 *Statistical Models in S* 2:309-376.
- 558 62. R-Core-Team (2020) R: A language and environment for statistical computing.
559 (R Foundation for Statistical Computing, Vienna, Austria).
- 560 63. Antoine D, Hillson S, & Dean MC (2009) The developmental clock of dental
561 enamel: a test for the periodicity of prism cross-striations in modern humans and
562 an evaluation of the most likely sources of error in histological studies of this
563 kind. *Journal of Anatomy* 214:45-55.
- 564 64. Dean MC (2006) Tooth microstructure tracks the pace of human life-history
565 evolution. *Proceedings of the Royal Society of London B: Biological Sciences*
566 273(1603):2799-2808.

- 567 65. Hillson S (2014) *Tooth development in human evolution and bioarchaeology*
568 (Cambridge University Press, Cambridge).
- 569 66. Lacruz RS, *et al.* (2012) The circadian clock modulates enamel development.
570 *Journal of Biological Rhythms* 27(3):237-245.
- 571 67. Zheng L, *et al.* (2013) Circadian rhythms regulate amelogenesis. *Bone* 55(1):158-
572 165.
- 573 68. Dean MC (1987) Growth layers and incremental markings in hard tissues; a
574 review of the literature and some preliminary observations about enamel structure
575 in *Paranthropus boisei*. *Journal of Human Evolution* 16(2):157-172.
- 576 69. Nava A, Frayer DW, & Bondioli L (2019) Longitudinal analysis of the
577 microscopic dental enamel defects of children in the Imperial Roman community
578 of Portus Romae (necropolis of Isola Sacra, 2nd to 4th century CE, Italy). *Journal*
579 *of Archaeological Science: Reports* 23:406-415.
- 580 70. Witzel C, *et al.* (2006) Reconstructing impairment of secretory ameloblast
581 function in porcine teeth by analysis of morphological alterations in dental
582 enamel. *Journal of Anatomy* 209(1):93-110.
- 583 71. Sabel N, *et al.* (2008) Neonatal lines in the enamel of primary teeth—a
584 morphological and scanning electron microscopic investigation. *Archives of Oral*
585 *Biology* 53(10):954-963.
- 586 72. Zanolli C, Bondioli L, Manni F, Rossi P, & Macchiarelli R (2011) Gestation
587 length, mode of delivery, and neonatal line-thickness variation. *Human Biology*
588 83(6):695-713.
- 589 73. Guatelli-Steinberg D, Floyd BA, Dean MC, & Reid DJ (2012) Enamel extension
590 rate patterns in modern human teeth: two approaches designed to establish an
591 integrated comparative context for fossil primates. *Journal of Human Evolution*
592 63(3):475-486.
593

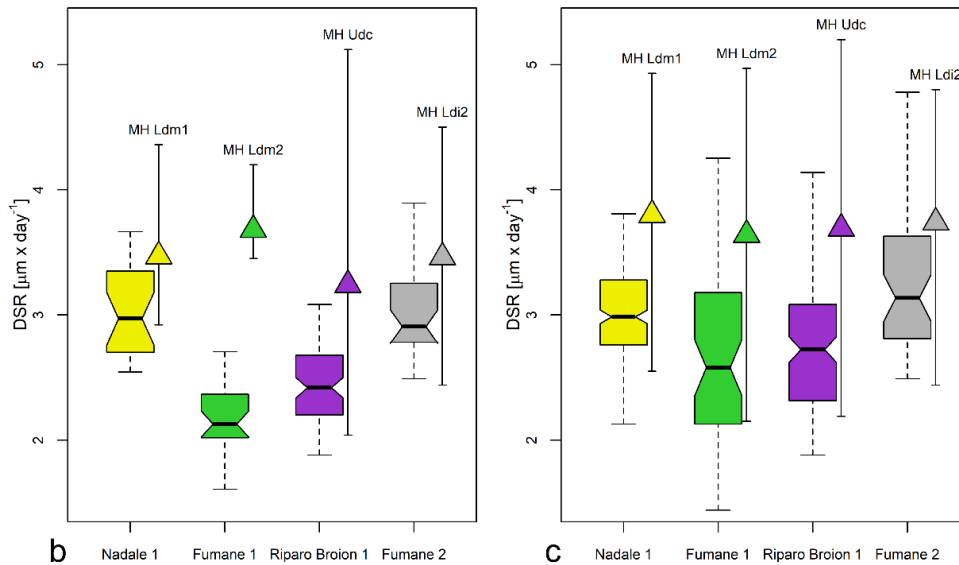
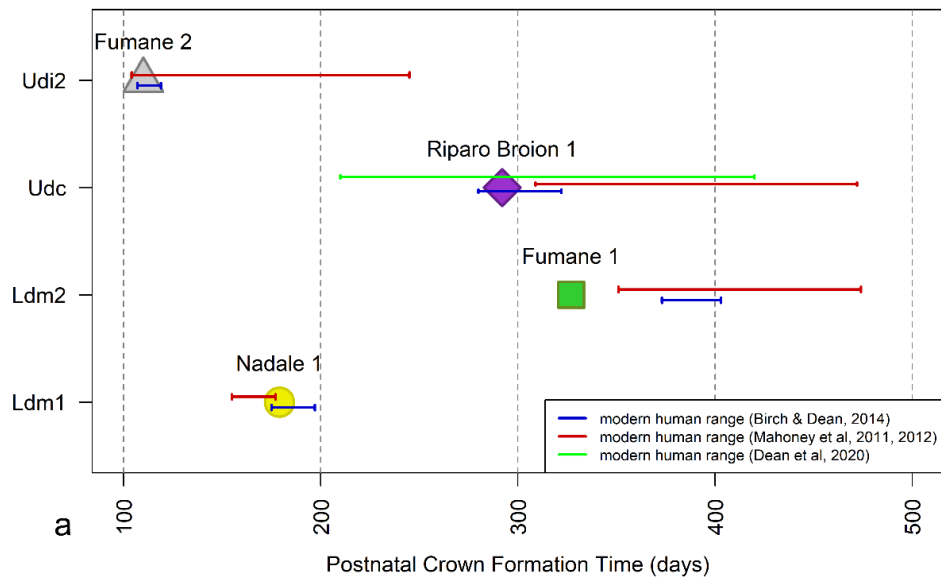
Figures and Tables



597
598

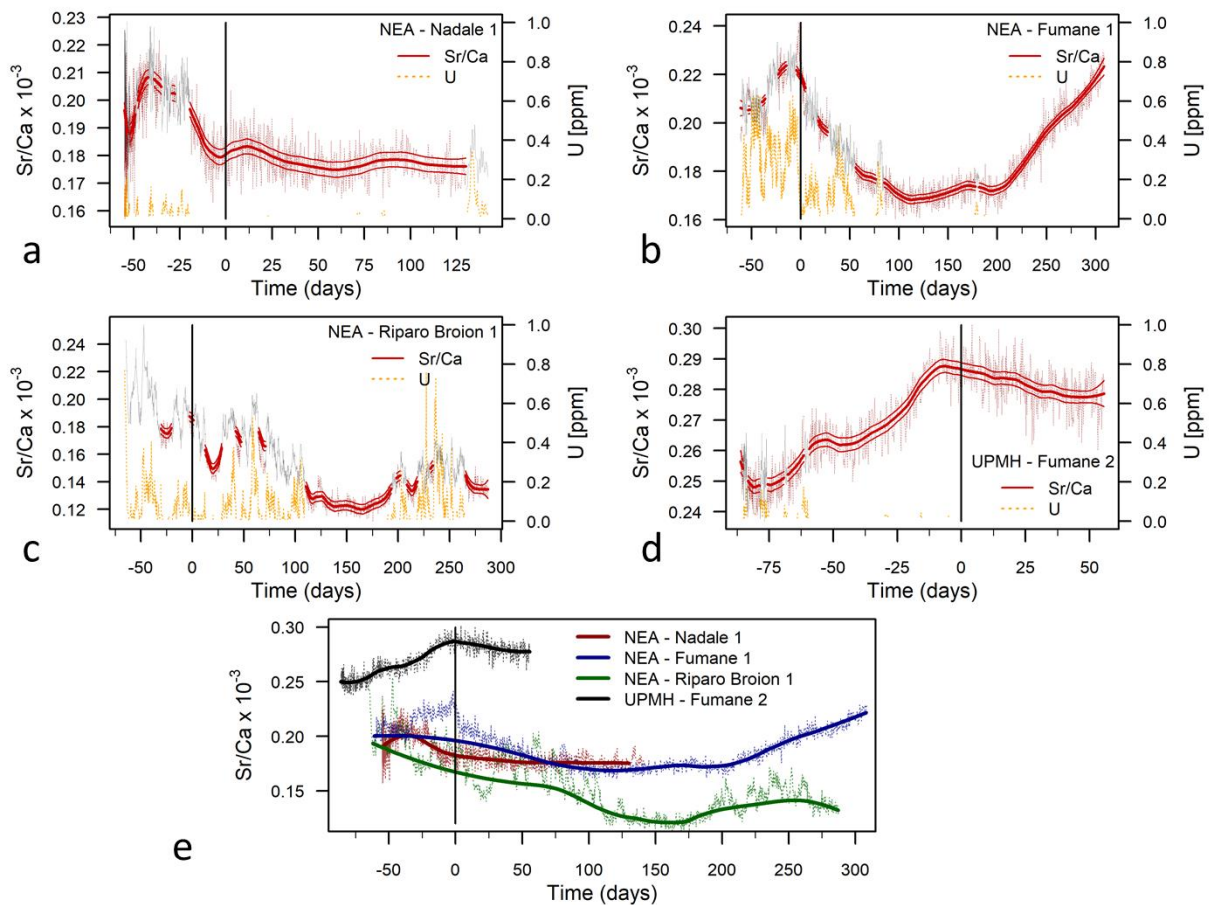
599 **Figure 1. Geographical, paleoecological and chronological framework.** (a) Oxygen
600 isotope curve from NGRIP (21), with Greenland Stadials 5-21 highlighted.
601 Chronologies of the human specimens are also reported (see Supplementary
602 Information for details); Fumane 2 is UPMH (green), while Fumane 1, Riparo
603 Broion 1 and Nadale 1 are Neanderthals (yellow). (b,c,d) Modelled Alpine glacier
604 extent during the time intervals of the teeth recovered at the sites of Fumane Cave
605 (b,c), Riparo Broion (c) and Nadale (d); location within Italy is shown in the inset.
606 Simulations show a high temporal variability in the total modelled ice volume
607 during Marine Isotope Stages 4 (70 ka snapshot) and 3 (50, 40 ka snapshots) with
608 glaciers flowing into the major valleys and possibly even onto the foreland (22).

609
610



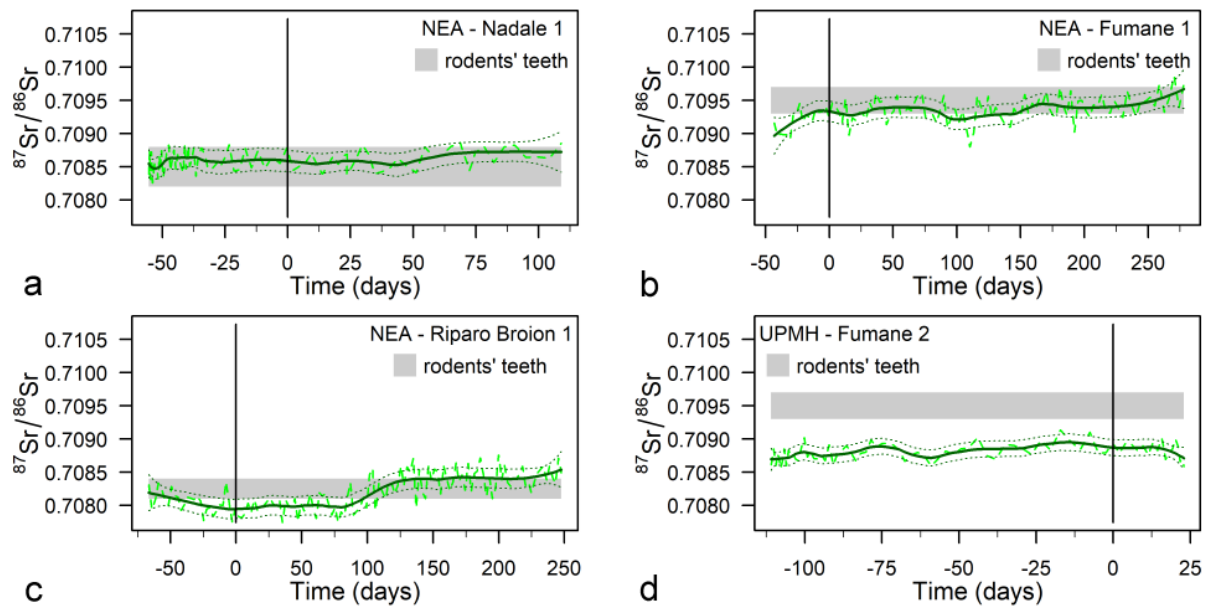
611

612 **Fig. 2. Dental crown growth parameters.** (a) Postnatal crown formation time in days
 613 from birth for the different deciduous teeth. The range of variability reported in
 614 literature for modern and archaeological individuals is represented by red, blue,
 615 green lines. (b) Boxplot of the daily secretion rate (DSR) variation in the first 100
 616 μm from the enamel-dentine-junction (min, second quartile, median, third quartile,
 617 max) and range of variation (min, mean, max) of modern humans (MH), re-
 618 assessed from (36-39). (c) Boxplot of the daily secretion rate variation across the
 619 whole crown (mean, second quartile, median, third quartile, max) and range of
 620 variation (min, mean, max) of modern humans (MH), re-assessed from (36-39).
 621 Ldm1 = lower deciduous first molar; Ldm2 = lower deciduous second molar; Udc
 622 = upper deciduous canine; Ldi2 = lower deciduous later incisor.



623

624 **Fig. 3. Nursing histories from time-resolved Sr/Ca variation in Middle-Upper**
 625 **Paleolithic deciduous teeth.** UPMH = Upper Paleolithic modern human; NEA =
 626 Neanderthal. The elemental profiles were analyzed within enamel close to the enamel-
 627 dentine-junction (EDJ); [U] is reported as the most sensitive proxy for diagenetic
 628 alteration (14) (see *SI Appendix*, Text S4). Grey portions of the profiles represent
 629 diagenetically overprinted enamel domains, based on elevated U concentrations. The
 630 birth event is highlighted by a vertical line. (a) Nadale 1: the slight decrease of Sr/Ca
 631 indicates exclusive breastfeeding until the end of crown formation (4.7 months); (b)
 632 Fumane 1: Sr/Ca variation indicates breastfeeding until 4 months of age (fully
 633 comparable with MCS1 sample, see Supplementary Figure S6); (c) Riparo Broion 1:
 634 Sr/Ca profile indicates exclusive breastfeeding until 5 months of age; (d) Fumane 2: 55
 635 days of available postnatal enamel shows exclusive breastfeeding. (e) Individual Sr/Ca
 636 profiles adjusted to the birth event; the interpolated modelled profiles were calculated
 637 based on those portions unaffected by diagenesis ($U < \text{limit of detection, } 0.012 \text{ ppm}$), with
 638 strong smoothing parameters to enhance the biogenic signal. See Material and Methods
 639 section for details.
 640



641

642 **Fig. 4. Mobility of the Middle-Upper Paleolithic infants via time-resolved $^{87}\text{Sr}/^{86}\text{Sr}$**
 643 **profiles of their deciduous teeth.** Grey horizontal bands represent the local Sr isotopic
 644 baselines defined via the Sr isotopic composition of archaeological rodent enamel (*SI*
 645 *Appendix*, Table S1). The birth event is indicated by a vertical line. (a,b) Nadale 1 /
 646 Fumane 1: exploitation of local food resources through the entire period; (c) Riparo
 647 Broion 1: possible limited seasonal mobility (non-local values between c. 25 and 75 days
 648 = 4 months); (d) Fumane 2: exploitation of non-local food resources through the entire
 649 period.

650

651

652

653

654

655

656

657 Supplementary Information for **Early life of Neanderthals**

658

659 Alessia Nava, Federico Lugli, Matteo Romandini, Federica Badino, David Evans, Angela
660 H. Helbling, Gregorio Oxilia, Simona Arrighi, Eugenio Bortolini, Davide Delpiano,
661 Rossella Duches, Carla Figus, Alessandra Livraghi, Giulia Marciani, Sara Silvestrini,
662 Anna Cipriani, Tommaso Giovanardi, Roberta Pini, Claudio Tuniz, Federico Bernardini,
663 Irene Dori, Alfredo Coppa, Emanuela Cristiani, Christopher Dean, Luca Bondioli, Marco
664 Peresani, Wolfgang Müller, Stefano Benazzi

665

666

667 To whom correspondence may be addressed. Email: alessia.nava@uniroma1.it;
668 federico.lugli6@unibo.it; marco.peresani@unife.it; w.muller@em.uni-frankfurt.de;
669 stefano.benazzi@unibo.it

670

671

672 **This PDF file includes:**

673

674 Supplementary text S1 to S4

675 Figures S1 to S13

676 Tables S1 to S3

677 Legends for Datasets S1 to S3

678 SI References

679

680 **Other supplementary materials for this manuscript include the following:**

681

682 Datasets S1 to S3

683

684

685 **SUPPLEMENTARY INFORMATION TEXT S1: DENTAL MORPHOLOGY**

686

687 The deciduous dental sample here investigated consists of three Neanderthals and one
688 Upper Paleolithic modern humans (UPMH) specimen.

689 Fig. S2 reports the surface rendering of the four teeth from high resolution
690 microtomographic volumes, segmented with Avizo 9.2 (Thermo Fisher Scientific). High-
691 resolution micro-CT images of Fumane 1 and 2 were obtained with a Skyscan 1172
692 microtomographic system using isometric voxels of 11.98 μm (Fumane 1 and Fumane 2)
693 (see Benazzi et al (1) for details). High-resolution micro-CT images of Nadale 1 and
694 Riparo Broion 1 were acquired with the Xalt micro-CT scanner using isometric voxels of
695 18.4 μm (see Arnaud et al (2) for details).

696 The Neanderthal specimen Nadale 1 is a lower right first deciduous molar (Fig. S1a),
697 whose morphological description and morphometric analysis were provided by Arnaud et
698 al (2). The taxonomical assessment of the Neanderthal tooth Fumane 1, a lower left
699 second deciduous molar (Fig. S1b), was confirmed by metric data and non-metric dental
700 traits (1), while the attribution of Fumane 2, an upper right lateral deciduous incisor (Fig.
701 S1d), to modern human was based on mitochondrial DNA (3).

702 The specimen Riparo Broion 1 is unpublished, but the paper describing its morphology
703 and morphometry is under review. Overall, Riparo Broion 1 is an exfoliated upper right
704 deciduous canine (Fig. S1c), heavily worn, with about one-fourth of the root preserved,
705 which suggests an age at exfoliation at about 11-12 years based on recent human
706 standards (4). The tooth is characterized by a stocky crown, bulging buccally, and a
707 distolingual projection of a lingual cervical eminence, ultimately producing an
708 asymmetrical outline. Overall our data concur to align Riparo Broion 1 to Neanderthals.

709 Overall, considering the paucity of European human remains dating to the Middle to
710 Upper Paleolithic transition, the dental sample here investigated represents a unique
711 exception for 1) its provenance from a restricted region of northeast Italy, ultimately
712 removing the geographical variable as a potential confounding factor for
713 chemical/isotopic signatures, 2) being represented by deciduous teeth, thus allowing to
714 evaluate diet and mobility during early infancy, 3) the presence of both late Neanderthal

715 specimens (Fumane 1 and Riparo Broion 1) and one of the earliest modern humans in
716 Europe (Fumane 2), thus providing a unique opportunity to compare subsistence
717 strategies between the two human groups around the time of Neanderthal demise.
718

719 **SUPPLEMENTARY INFORMATION TEXT S2: ARCHAEOLOGICAL AND**
720 **PALEOENVIRONMENTAL CONTEXTS**

721

722 Nadale 1

723 De Nadale Cave is a small cavity located 130m a.s.l. in the middle of the Berici Hills.
724 Research at De Nadale Cave started in 2013 when a first excavation campaign led to the
725 discovery of a cave entrance after the removal of reworked sediments. Later, six
726 campaigns were carried out between 2014 and 2017 in order to investigate the deposits
727 preserved in the cave entrance and the back (5). The excavations exposed a stratigraphic
728 sequence which includes a single anthropic layer (unit 7) embedded between two sterile
729 layers (units 6 and 8) partly disturbed by some badger's dens along the cave walls. Unit 8
730 lays on the carbonate sandstone bedrock. Besides these disturbances, unit 7 is well
731 preserved and extends into the cavity. It yielded thousands of osteological materials,
732 lithic implements, and the Neanderthal deciduous tooth (2). A molar of a large-sized
733 ungulate was U/Th dated to 70,200±1,000/900 years as a minimum age (5) placing the
734 human occupation to an initial phase of the MIS 4. The zooarchaeological assemblage is
735 largely ascribable to human activity (6). Neanderthals hunted and exploited mainly three
736 taxa: the red deer (*Cervus elaphus*), the giant deer (*Megaloceros giganteus*) and bovids
737 (*Bison priscus* and *Bos primigenius*) (6, 7), in association with other taxa consistent with
738 the paleoclimatic and paleoenvironmental reconstruction based on the small mammal
739 association, where the prominence of *Microtus arvalis* identifies a cold climatic phase
740 and correlates to a landscape dominated by open woodlands and meadows (8). A large
741 amount of anthropic traces is observed on the ungulate remains, ascribable to different
742 stages of the butchery process and to the fragmentation of the bones for marrow
743 extraction. Burnt bone fragments and charcoal accumulations have been likely related to
744 residual fire-places (6). Lithic industry from of De Nadale differentiates technologically
745 and typologically from the Mousterian elsewhere in the region, especially with regard to
746 the core reduction methods and the types of flakes and retouched tools. These are
747 represented from several scrapers with stepped-scaled invasive retouches and make the

748 De Nadale industry comparable to Quina assemblages in Italy and Western Europe (5).
749 De Nadale peculiarity is also enhanced by the high number of bone retouchers (9).
750 Research at the De Nadale Cave is coordinated by the University of Ferrara (M.P.) in the
751 framework of a project supported by the Ministry of Culture – “SABAP per le province
752 di Verona, Rovigo e Vicenza” and the Zovencedo Municipality, financed by the H.
753 Obermaier Society (2015), local private companies (R.A.A.S.M., Saf and Lattebusche),
754 and local promoters.

755

756 Fumane 1 and 2

757 Grotta di Fumane (Fumane Cave) is a cave positioned at the western fringe of the Lessini
758 plateau in the Venetian Pre-Alps. The site preserves a finely layered late Middle and early
759 Upper Paleolithic sequence with evidence of cultural change related to the demise of
760 Neanderthals and the arrival of the first Anatomically Modern Humans (3, 10-12). Teeth
761 Fumane 1 and Fumane 2 were found in Middle Paleolithic unit A11 and Upper
762 Paleolithic unit A2 associated to Mousterian and Aurignacian cultures respectively.

763 Of the late Mousterian layers, unit A11 is a stratigraphic complex composed of an
764 ensemble of thin levels with hearths that was surveyed in different years at the eastern
765 entrance of the cave over a total area of 10 sqm. The chronometric position of A11 is
766 provided by only one U/Th date to $49,000 \pm 7,000$ years for level A11a, given unreliability
767 to the radiocarbon dataset currently available (13) but see (14). New radiocarbon
768 measurements are in progress. Paleoecological indexes calculated on the composition of
769 the micromammal assemblage point for a temperate and relatively moist period related to
770 an interstadial before HE5 (15), in a landscape dominated from open-woodland
771 formations in accordance with the previous indications based on the zooarchaeological
772 assemblage. Cervids (red deer, giant deer and roe deer) largely prevail on bovids and
773 caprids (ibex and chamois) and other mammal species (16). No taphonomic analyses
774 have still been conducted to confirm the anthropogenic nature of the accumulation of the
775 animal bone remains. Lithic artifacts belong to the Levallois Mousterian. The use of this
776 technology is recorded by high number of flakes, cores and by-products shaped into

777 retouched tools like single and double scrapers, also transverse or convergent and few
778 points and denticulates (11).

779 Aurignacian layer A2 records an abrupt change in material culture represented from lithic
780 and bone industry (10, 17, 18), beads made of marine shells and bone (10, 19), use of red
781 mineral pigment (20). Bone and cultural remains have been found scattered on a
782 paleoliving floor with fire-places, toss zones and intentionally disposed stones (21). A
783 revised chronology of the Mid-Upper Paleolithic sequence (14) has shown that the start
784 and the end of level A2 date respectively to 41,900-40,200 cal BP and 40,300-39,400 cal
785 BP at the largest confidence interval. Macro- and micro-faunal remains show an
786 association between forest fauna and cold and open habitat species typical of the alpine
787 grassland steppe above the tree line in a context of climatic cooling (15, 22, 23). Hunting
788 was mostly targeted adult individuals of ibex, chamois and bison and occurred
789 seasonally, from summer to fall (22, 24).

790 Research at Fumane is coordinated by University of Ferrara (M.P.) in the framework of a
791 project supported by the Ministry of Culture – “SABAP per le province di Verona,
792 Rovigo e Vicenza”, public institutions (Lessinia Mountain Community - Regional
793 Natural Park, Fumane Municipality, BIMAdige, SERIT) and by private institutions,
794 associations and companies. Research campaigns 2017 and 2019 have received funding
795 from the European Research Council (ERC) under the European Union’s Horizon 2020
796 research and innovation programme (grant agreement No 724046 – SUCCESS,
797 <http://www.erc-success.eu>).

798 Riparo Broion 1

799 The Berici Mounts are a carbonatic karst plateau at low altitude at the southern fringe of
800 the Venetian Pre-Alps in the Alpine foreland. This is a large alluvial plain that was
801 formed initially during the Middle and Late Pleistocene by a number of major rivers,
802 including the Po, the Adige and those of the Friulian-Venetian plain. The western zone of
803 the Berici is a gentle landscape which conjoins to the alluvial plain. Conversely, along its
804 eastern slope the plateau connects abruptly to the alluvial plain. Here, caves and
805 rockshelters have been archaeologically investigated since the XIX century up to present
806 days by teams from the University of Ferrara. Of these cavities, Riparo del Broion is a

807 flagship site for the late Middle and early Upper Paleolithic in this area. It is situated at
808 135m a.s.l. at the base of a steep cliff of Mount Brosimo (327 m a.s.l.) along a terraced
809 slope for cultivation during recent historical times. The shelter is 10m long, 6m deep and
810 17m high and originated from rock collapse along a major ENE-WSW oriented fault that
811 developed from thermoclastic processes and chemical dissolution comparably to other
812 cavities in the area (25, 26). Two additional Paleolithic cavities were investigated on the
813 western side of the same cliff, Grotta del Buso Doppio del Broion and Grotta del Broion
814 (27, 28).

815 The sedimentary deposits of Riparo Broion were partially dismantled in historical times
816 by shepherds with use to store hay and wood. Further damage occurred in 1984 when
817 unauthorized excavators removed sediments from pits and trenches on a total area of
818 14sqm down to 2m at the deepest. Archaeological excavations were initially directed by
819 Alberto Broglio (1998 -2008) and by two of us (M.P. and M.R.) in 2015 on a 20sqm area
820 bounded to north and west from the rock walls. Faunal remains and Middle and Upper
821 Paleolithic (Uluzzian, Gravettian and Epigravettian) cultural material was uncovered (29-
822 31). The bedrock has not yet been reached. Sediments are mostly small stones and gravel
823 with large prevalence on loams: 16 stratigraphic units planarly bedded have been
824 identified. The lowermost (11, 9, 7 and 4) contain Mousterian artefacts, faunal remains
825 and clearly differentiate in dark-brownish color from the other units.

826 The human canine was discovered in unit 11 top. This unit has been ¹⁴C dated to
827 48,100±3100 years BP with range from 50.000 to 45.700 years cal BP as the most likely
828 age (31). Stone tools are too low in number to propose an attribution to one or another
829 Mousterian cultural complex. Preliminary zooarchaeological data report a variety of
830 herbivores such as elk, red deer, roe deer, megaceros, wild boar, auroch/bison, a few
831 goats and horses, and common beaver associated sparse remains of fish and freshwater
832 shells. This association reflects the presence of a patchy environmental context, with
833 closed to open-spaced forests, Alpine grasslands and pioneer vegetation complemented
834 by humid-marshy environments and low-energy water courses, wet meadows and shallow
835 lacustrine basins.

836 Research at Riparo Broion is coordinated by the Bologna (M.R.) and Ferrara (M.P.)
837 Universities in the framework of a project supported by the Ministry of Culture –
838 “SABAP per le province di Verona, Rovigo e Vicenza”, public institutions (Longare
839 Municipality), institutions (Leakey Foundation, Spring 2015 Grant; Istituto Italiano di
840 Preistoria e Protostoria). Research campaigns 2017-2019 have received funding from the
841 European Research Council (ERC) under the European Union’s Horizon 2020 research
842 and innovation programme (grant agreement No 724046 – SUCCESS, [http://www.erc-
843 success.eu](http://www.erc-success.eu)).

844

845 Paleoenvironmental contexts

846 The paleoenvironmental contexts during the time intervals of the teeth recovered at the
847 sites of Nadale, Fumane cave and Riparo Broion (~ 70, 50 and 40 ka) can be inferred on
848 the basis of two high-resolution paleoecologically records from NE-Italy: Lake Fimon
849 (Berici Hills) and Palughetto basin (Cansiglio Plateau, eastern Venetian Pre-Alps). Pie
850 charts presented in Fig. S3 show the relative abundances of different vegetation types at
851 5000 years’ time-slice intervals. Pollen % are calculated based on the sum of terrestrial
852 taxa and represent mean values. Pollen taxa are grouped according to their ecology and
853 climatic preferences. Eurythermic conifers (EC): sum of *Pinus* and *Juniperus*; Temperate
854 forest (TF): sum of deciduous *Quercus*, *Alnus glutinosa* type, *Fagus*, *Acer*, *Corylus*,
855 *Carpinus*, *Fraxinus*, *Ulmus*, *Tilia* and *Salix*; Xerophytic steppe (XS): sum of *Artemisia*
856 and *Chenopodiaceae*. Other herbs: sum of terrestrial herbs, *Chenopodiaceae* excluded.
857 Original pollen data used for % calculation for the Palughetto basin are from (32).

858 On a long-term scale, the paleoecological record from Lake Fimon points to persistent
859 afforestation throughout the Early to Middle Würm in the Berici Hills (i.e., Nadale,
860 Fumane and Riparo Broion sites). Moderate forest withdrawals occurred during
861 Greenland stadials (GSs), possibly enhanced during GSs hosting Heinrich Events (HEs)
862 (33).

863 Between 75 and 70 ka, at the end of the second post-Eemian interstadial, the landscape
864 was dominated by a mosaic of boreal forests with eurythermic conifers (46%) and

865 subordinated temperate taxa (10%). Open environments are identified by pollen of
866 herbaceous taxa and steppe/desert forbes-shrubs (23%).
867 During the 50-45 ka and 45-40 ka time-slices, steppic communities further increase (7-
868 8%) as a result of enhanced dry/cold conditions during Greenland stadials (GSs). Pollen
869 of eurythermic conifers sum up to 37-38%. Temperate trees, notably *Tilia*, persisted in
870 very low percentages (4%) up to ~40 ka (34).
871

872 **SUPPLEMENTARY INFORMATION TEXT S3: TOWARDS A CONCEPTUAL**
873 **MODEL FOR Sr/Ca AND Ba/Ca BEHAVIOR IN HUMAN INFANTS:**
874 **THEORETICAL FRAMEWORK AND EMPIRICAL EVIDENCE FROM**
875 **CONTEMPORANEOUS INFANTS WITH KNOWN FOOD INTAKE**

876 Strontium and barium are non-bioessential trace elements with no major metabolic
877 functions in the human body. Strontium and Ba mimic Ca, given their coherent behavior
878 as alkaline earth elements with respect to their divalent charge, but are characterized by
879 larger ionic radii (Sr: 1.18, Ba: 1.35, Ca: 1.00 Å (10^{-10} m)); (35). Overall, they both follow
880 the Ca metabolism but due to their larger ionic size are discriminated against in the
881 gastrointestinal tract (GIT) (36, 37). Given the larger size, Ba is even more strongly
882 discriminated against relative to Sr (37, 38). Similarly, kidneys tend to excrete Sr and Ba
883 more rapidly compared to Ca (39). From plasma, Sr, Ba and Ca are mainly fixed in bones
884 and teeth with a likely further bias in favor of Ca (39, 40). Taken together, these factors
885 cause Ca-normalized concentrations of Sr and Ba in skeletal tissues to be lower than
886 those of the diet, a process known as ‘biopurification’ (36). Burton and Wright (41)
887 demonstrated that Sr/Ca of bones is approximately 5 times lower than the respective
888 Sr/Ca value of the diet. Such evidence has been also demonstrated empirically by many
889 studies (36-38, 42, 43). These pioneering studies also emphasized that Sr/Ca and Ba/Ca
890 might be used as tools for paleodiet and trophic chain reconstruction (36).

891 Interestingly, significant GIT discrimination of Sr and Ba over Ca ions progressively
892 increases during human growth and becomes significant at around one year of age (44,
893 45). This hints that both the Sr/Ca and Ba/Ca ratios of infant plasma (<1 year) should be
894 closer to the value of their respective dietary inputs (46). Indeed, Lough et al (46)
895 demonstrated that the relative ratio between body Sr/Ca and dietary Sr/Ca for an infant is
896 ~0.90. Hence, for example, in breast-fed infants, the Sr/Ca of their blood plasma should
897 reflect the Sr/Ca of the consumed breastmilk. Studies of elemental transport in humans
898 have shown that Ca is actively transported (47), resulting in lower Sr/Ca ratios in both
899 umbilical cord sera and breastmilk than in mother sera due to the larger size of Sr ions
900 compared to Ca ions. Yet, empirical evidence indicates that mammary gland
901 discrimination for Sr (2.5-fold) is higher than placenta (1.7-fold), yielding average

902 breastmilk Sr/Ca values lower than umbilical cord (fetal) values (48). Crucially, fetal
903 blood chemistry is recorded in prenatal dental enamel and breastmilk consumption in
904 postnatal enamel and can be reconstructed via high-spatial resolution chemical analysis of
905 teeth (49, 50). Thus, higher Sr/Ca signals in prenatal domains followed by lower
906 postnatal Sr/Ca indicate breastmilk consumption (see Fig. S4). This has been previously
907 shown by the Sr/Ca distribution in teeth (50, 51), but also in elemental analyses of sera
908 samples. Krachler et al. (52) showed that Sr/Ca levels are two times higher in umbilical
909 cord sera than in breast-fed infant sera. On the other hand, due to the nominal lower
910 trophic level of herbivores, their milk has higher Sr/Ca than human milk. Hence, when a
911 child is fed through formula (largely based on cow milk), a Sr/Ca increase in the
912 postnatal enamel is expected (Fig. S4).

913 Indeed, Krachler et al. (52) reported high Sr/Ca values in formula-fed infant sera.
914 Moreover, a compilation of published Sr/Ca data of geographically dispersed human and
915 bovine/caprine milks (Fig. S5 and references in caption) indicates that human breastmilk
916 has a rather homogeneous Sr/Ca ratio of $\sim 0.1 \pm 0.01 \cdot 10^{-3}$, 4 times lower than non-human
917 milk and formula ($\sim 0.39 \pm 0.15 \cdot 10^{-3}$).

918 From all these inferences, the Sr/Ca ratio of both breast-fed and formula-fed infants can
919 be modelled relative to an initial Sr/Ca mother diet, set equal to 1 (Tab. S2 and Fig. S4).
920 With the introduction of transitional food in the infant diet, a change in Sr/Ca values is
921 also expected. If the child was initially breast-fed, one should predict an increase of the
922 Sr/Ca ratio during transitional feeding, because both meat and especially vegetables
923 retain higher Sr/Ca than breastmilk (see e.g. 53). In general, an increased Sr/Ca signal
924 from transitional foods is also expected for formula-fed babies. However, due to the
925 compositional variability of some formulas (e.g. soy-based) and non-human milk, a
926 decrease of the Sr/Ca ratio may occur if a highly-biopurified food (e.g. close to human
927 milk) is used for initial weaning.

928 Contrary to strontium, a reliable interpretation of Ba/Ca data is difficult due to
929 contradictory literature and the lack of studies on Ba metabolism. Austin et al. (54)
930 suggested that the increased level of both Sr/Ca and Ba/Ca ratios in breast-fed infants
931 reflected improved Sr and Ba absorption during breastfeeding. Such an increase in Sr/Ca

932 is in stark contrast to any other study on breastfed children (49, 50). Similarly, Krachler
933 et al. (55) highlighted increased levels of Ba/Ca in colostrum and breast-fed infant sera
934 compared to umbilical cord sera (Tab. S3). However, colostrum is not a good proxy for
935 breastmilk elemental content, being highly enriched in metals (56, 57). In fact, when
936 compared with Sr/Ca and Ba/Ca ratios from literature, colostrum values reported in
937 Krachler et al. (55) are about 2 times higher than other human milk samples (Figure S5).
938 Moreover, other studies suggested that only a very limited portion of the absorbed Ba
939 (~3%) is transferred to the breast-milk (48).

940 Studies of dental enamel indicate that Ba overall behaves akin to Sr (50, 53, 58, 59),
941 decreasing with breastmilk consumption and increasing along with the introduction of
942 transitional food. Still, Müller et al. (50) noted that Ba behavior in tooth enamel is less
943 predictable than Sr. This observation may also relate to the high variability of Ba content
944 in human milk, colostrum and formulas (see (55) and Fig. S5). Notably, Taylor et al. (60)
945 pointed out that in controlled-fed rats, the consumption of cow milk leads to an increase
946 of Ca absorption, without changing the Ba absorption. This, in turn, corroborates the idea
947 that the relative Ba/Ca ratio in rats should decrease with a milk-based diet and increase
948 with a non-milk diet. In the same publication, the authors reported that Ba absorption
949 increased two-fold in young starved rats, whereas Ca absorption decreased in the same
950 individuals, pointing towards an association of Ba/Ca with dietary stress rather than
951 weaning transitions.

952 Around one year of age, both Ba/Ca and Sr/Ca gradually decrease due to the progressive
953 increase in GIT discrimination in the infant due to a preferential absorption of Ca relative
954 to Sr and Ba (44, 45). Taken together, we conclude that models for Sr/Ca with respect to
955 dietary transitions in early life have a stronger theoretical basis compared to Ba.

956

957 The modern reference sample

958 In the following we present spatially-resolved chemical data from contemporaneous
959 individuals with known dietary behavior to evaluate the theoretical framework presented
960 above. To avoid the problem of retrospectively reporting breastfeeding and weaning
961 practice (61), we selected offspring from parents who reliably took and preserved notes

962 of the feeding practice during the nursing period (explicit written consent was obtained
963 by all relevant people with legal authority). All individual data were treated in a fully
964 anonymous way and it is not possible from the present results to identify the involved
965 individuals.

966 Three deciduous teeth, representing three different nursing histories, were analyzed by
967 LA-ICPMS: an exclusively breastfed individual from Switzerland (deciduous second
968 molar dm2; MCS1), an exclusively bottle-fed individual from central Italy (deciduous
969 canine dc; MCS2 previously published as MOD2 in (50)), a mixed breast-/bottle-fed
970 individual from central Italy (deciduous canine dc; MCS3). The mothers of the three
971 infants did not travel for extended periods during the interval in which these deciduous
972 teeth were forming.

973 MCS1 is a lower deciduous second molar from an individual exclusively breastfeed until
974 the fifth month of life (154 days; Fig. S6). No supplementary food was given to the infant
975 during this period. The Sr/Ca profile analyzed parallel to the enamel-dentine junction
976 (EDJ) shows a constant decrease in the elemental ratio until ~154 days corresponding to
977 the reported period of exclusive breastfeeding. Just after the introduction of solid food
978 once a day (reported from day 155), the slope of the profile becomes gradually shallower,
979 particularly, this was coincident with the introduction of some formula milk (reported
980 from day 182). Fifteen days after cutting down breastfeeding during daytime (reported on
981 day 209) the profile begins to show a sharp increase of the Sr/Ca values. At 8.5 months of
982 life (reported on 258 days) the breastfeeding period of individual MCS1 stopped and the
983 diet continued with solid food and formula milk. The rather flat Sr/Ca signal observed in
984 the last part of the profile (after day ~340) likely reflects the effects of maturation-
985 overprint due to the thin enamel closest to the crown neck (50). The striking
986 correspondence of the independently recorded dietary transitions in MCS1 with the Sr/Ca
987 trend fully supports the use of Sr/Ca as a proxy for making nursing events. In this sense,
988 based on modelled values reported in Tab. S2, the theoretical ratio between Sr/Ca in
989 prenatal enamel and breastfeeding signal is ~0.7. In MCS1, this ratio is ~0.8, indicating a
990 remarkable correspondence between the theoretical model and the observed data. The
991 MCS1 Ba/Ca profile broadly follows the trend observed for Sr/Ca, decreasing - with

992 proportionately smaller changes in Ba levels across lifetime - from birth until ~160 days.
993 Thereafter, Ba/Ca steadily increases till day 235, steeply increases until day ~290 (9.5
994 months) to then decrease again for 25 days. Finally, Ba/Ca constantly increases to the end
995 of the crown formation. This fluctuation in the last part of the profile cannot be explained
996 by any event in the known dietary/health history of MCS1.

997 MCS2 is a deciduous canine from an exclusively formula-fed individual (Fig. S7), whose
998 results have already been partially presented in the context of enamel mineralization
999 processes as MOD2 (50). The Sr/Ca profile, run parallel to the EDJ, shows a constant
1000 increase after birth until ~130 days (~4.3 months), and then it starts to decrease as a
1001 consequence of the combined effects of the onset of the reported transitional period and
1002 maturation overprint. The absolute values of Sr/Ca through all the postnatal period are
1003 higher than $5 \cdot 10^{-4}$ and thus higher than those observed in the other contemporary
1004 reference individuals (Figure S4b). The model reported in Fig. S4 and Table S2 specifies
1005 a ratio between prenatal enamel and formula Sr/Ca signal equal to ~2.2. In MCS2, this
1006 ratio is ~1.8, corroborating the hypothesis that with formula introduction the postnatal
1007 Sr/Ca should double. The Ba/Ca profile follows the same trend observed in the Sr/Ca
1008 profile, increasing from birth until ~75 days (2.5 months), then remaining stable with
1009 some fluctuation until ~175 days (5.8 months).

1010 MCS3 is an upper deciduous canine from a mixed breast- formula-fed individual (Fig.
1011 S8). This infant was exclusively breastfed for the first 30 days. After that, the mother
1012 complemented the infant diet with formula milk. Mixed feeding was carried on until 4
1013 months of age, at which time the mother underwent surgery. During this period of illness,
1014 the mother used a breast pump to continue breastfeeding. After the surgery, the mother
1015 continued to breastfeed the infant with formula milk supplements, until the onset of
1016 weaning at six months.

1017 The X/Ca profiles were nominally analyzed close to daily-resolution (6 μm spots vs. 10.3
1018 $\mu\text{m}/\text{day}$ mean enamel extension rate), well-reflecting this complex nursing history and
1019 almost perfectly matching the main dietary shifts. Ba/Ca mirrors the Sr/Ca pattern,
1020 decreasing during the period of exclusive breastfeeding, slightly increasing during the
1021 mixed breast- bottle-feeding, and increasing further at the onset of weaning. The Ba/Ca

1022 profile follows the main dietary shifts but with less precision than Sr/Ca. Moreover, as in
1023 MCS1, the period of exclusive breastfeeding is characterized by a sharp decrease in
1024 Ba/Ca, contrary to what expected by Austin et al. (54). We note here that the small laser
1025 spot (6 μm) used during analysis resulted in lower ICPMS signals and hence overall
1026 larger analytical variability than for the other two specimens.

1027

1028 The fossil Late Pleistocene human dental sample

1029 Nadale 1 - Neanderthal

1030 In Nadale1, Sr/Ca profile slightly decreases until the end of the crown, depicting a
1031 breastfeeding signal until the end of the crown formation. Unusually, Ba/Ca shows the
1032 opposite trend to Sr/Ca (Fig. S9), and appears to follow the dietary model proposed by
1033 (54). Mg/Ca is largely invariant across the whole crown, and only very minor diagenetic
1034 alteration is apparent via U peaks at the very beginning and end of the crown that have
1035 very limited correspondence in Ba/Ca and Sr/Ca.

1036

1037 Fumane 1 - Neanderthal

1038 In Fumane 1, the Ba/Ca profile broadly follows that of Sr/Ca (Fig. S10), yet especially
1039 for the first ~120 days displays several pronounced, narrow peaks that correlate positively
1040 with U and negatively with Mg, respectively. These reveal localized diagenetic overprint
1041 that is far less manifested for Sr/Ca. According to our model, Sr/Ca indicates an exclusive
1042 breastfeeding signal until 115 days (4 months), followed by the first introduction of non-
1043 breastmilk food and a stronger signal visible at 200 days (6.6 months), at which point
1044 there is a steep increase in Sr/Ca that likely indicates a more important and substantial
1045 introduction of supplementary food. This profile is fully comparable to the MCS1 pattern
1046 reported above. According to (54), this individual falls outside the bounds of their model,
1047 because a decrease in Ba/Ca after birth is never detected in their data.

1048

1049 Riparo Broion 1 - Neanderthal

1050 In Riparo Broion 1, the Ba/Ca profile overall varies in parallel (Fig. S11), but also shows
1051 some prominent peaks that correlate positively with U and negatively with Mg,

1052 respectively, indicating, similar to Fumane 1, that U uptake and Mg loss are indicators of
1053 localized diagenetic alteration (see Figure 3 main text). Regardless of diagenesis, both
1054 elemental ratios vary in the same way. According to our contemporary reference sample,
1055 a decrease in the Sr/Ca ratio is a consequence of exclusive breastfeeding until 160 days (5
1056 months), after which an increase in Sr/Ca points to the first introduction of non-
1057 breastmilk food.

1058

1059 Fumane 2 - Aurignacian

1060 The Ba/Ca profile of Fumane 2 follows that of Sr/Ca (Fig. S12), slightly decreasing in the
1061 first month of postnatal life and then increasing in the most cervical enamel. The short
1062 postnatal portion of available enamel (~55 days) precludes the chemical detection of the
1063 onset of weaning but a clear breast-feeding signal is detectable after birth since Sr/Ca
1064 decreases. Ba/Ca also decreases accordingly, and all is independent of diagenesis that is
1065 very low.

1066

1067 **SUPPLEMENTARY INFORMATION TEXT S4: ASSESSMENT OF POST-**
1068 **MORTEM DIAGENETIC ALTERATION OF BIOAPATITE**

1069

1070 In order to retrieve primary in-vivo elemental and isotopic signals from fossil teeth,
1071 preferably no alteration by post-mortem diagenetic processes should have taken place.
1072 During the post-depositional history, however, bioapatite may react with soils and
1073 underground waters, which can modify the initial biogenic chemical composition.
1074 Depending on apatite crystal-size, organic content and porosity, the distinct dental tissues
1075 behave differently in a soil environment. Bone and dentine are most susceptible to
1076 diagenetic chemical overprint, in contrast to highly-mineralized enamel (62-65). Equally,
1077 the extent of chemical overprint depends on the concentration gradient between burial
1078 environment and bioapatite tissue as well as the partition coefficient for the element(s)
1079 concerned.

1080 While alkali-earth elements (e.g. Ba, Mg and Sr) and biologically-important divalent
1081 metals (e.g. Cu, Fe and Zn) are present at mid-high concentrations (i.e. $>1 - 10^3 \mu\text{g/g}$) in
1082 modern bioapatite, Rare Earth Elements (REE), actinides and high-field strength
1083 elements (e.g. Hf, Th and U) have very low concentrations (lowest ng/g) in modern
1084 teeth/bones, yet are usually strongly incorporated into apatite during fossilization
1085 processes (66).

1086 In particular, uranium as water soluble (as uranyl $(\text{UO}_2)^{2+}$) and highly mobile element is
1087 readily incorporated into bioapatite (67, 68), such that uranium in fossil bioapatite,
1088 especially in bone and dentine, often shows high concentrations ($>10\text{s} - 100\text{s} \mu\text{g/g}$),
1089 whereas enamel frequently displays much lower U concentrations (e.g. (69)). Given these
1090 variations at the microscale, uranium can reveal diagenetic overprint in tandem with Mn
1091 or Al. Conversely, some bio-essential trace elements in bioapatite such as Mg may
1092 decrease post-mortem due to precipitation of diagenetic phases with lower trace metal
1093 concentrations, incipient recrystallization or leaching from the dental/bone tissue (70, 71).
1094 To monitor diagenetic alterations of our fossil dental specimens, we monitored ^{25}Mg ,
1095 ^{27}Al , ^{55}Mn , ^{89}Y , ^{140}Ce , ^{166}Er , ^{172}Yb and ^{238}U signals during the LA-ICPMS analyses and
1096 found that U (and Al) were the most sensitive indicators of diagenetic alteration, while

1097 commonly utilized REEs plus Y were rather insensitive in all cases as they remained at
1098 detection limit even in domains with clearly elevated U and Al. As a result, REE + Y are
1099 not shown here and we focus on U as main proxy for post-mortem diagenesis.

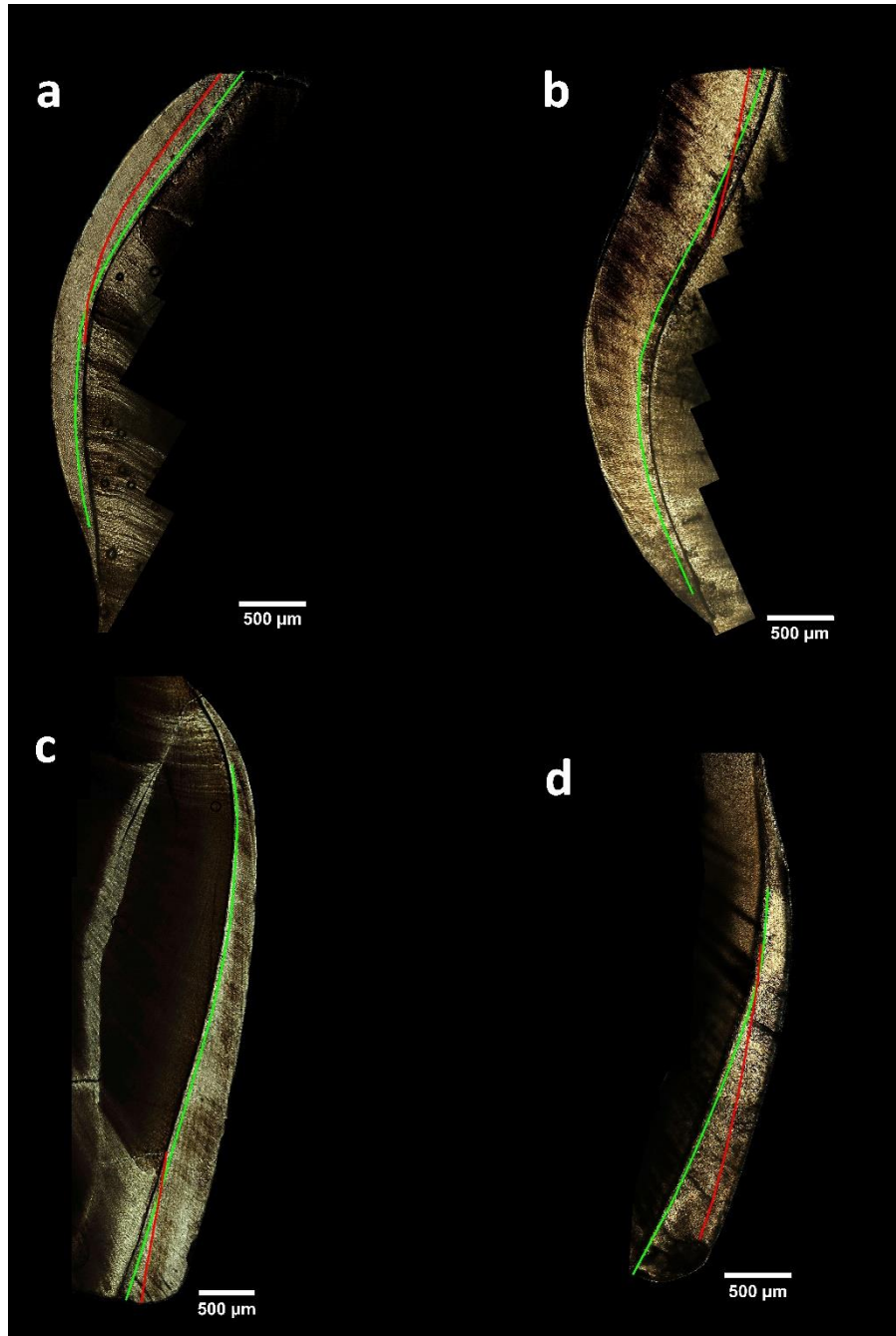
1100 Scatter plots between U and the residuals of Sr, Ba or Mg variation for the diagenetically
1101 most affected segments (Fig. S13) illustrate well the nature of element-specific diagenetic
1102 overprint of the four teeth. In samples with overall low [U] ($<0.2 \mu\text{g/g}$), i.e. Nadale 1 and
1103 Fumane 2, there are no significant positive or negative correlations discernible. In case of
1104 Riparo Broion 1 and Fumane 1, [U] rises up to $0.6 \mu\text{g/g}$ and positively correlates with Ba
1105 and negatively with Mg, while Sr only shows significant co-variation in Riparo Broion 1.
1106 It should be noted that spatially-resolved analysis by LA-ICPMS not only allows the
1107 retrieval of time-resolved chemical signals, but is equally ideally-suited for the
1108 delineation of well-preserved segments in partially diagenetically-overprinted samples.
1109 We employ the following strategy to delineate well-preserved from diagenetically
1110 overprinted segments in our enamel profiles:

1111 1) The visible co-variation between U and Sr/Ca (Fig. 3) as well as above mentioned
1112 correlations between Sr, Ba, Mg residuals with U (Fig. S13) show that especially Ba and
1113 less so Sr (only Riparo Broion 1) were added during diagenesis, while Mg was lost.
1114 Consequently, only data segments with lowest U ($[\text{U}] < \sim 0.05 \mu\text{g/g}$) were used for further
1115 considerations.

1116 2) The shape and nature of the discernible peaks/troughs provide an additional constraint.
1117 Very sharp variations, over less than 5 days, in U, Ba, Mg in Fumane 1 (Fig. S10) and U,
1118 Ba, Sr, Mg in Riparo Broion 1 (Fig. S11) characterize diagenetic signals, while variations
1119 in low-U domains are far more gradual and occur over tens of days. The latter is more in
1120 line with biologically-mediated variations that are additionally modulated by the
1121 protracted nature of enamel mineralization (50), which precludes, for example, the up to
1122 fourfold variability in Ba/Ca occurring at the profile start of Fumane 1 to be of in-vivo
1123 origin (Fig. S10).

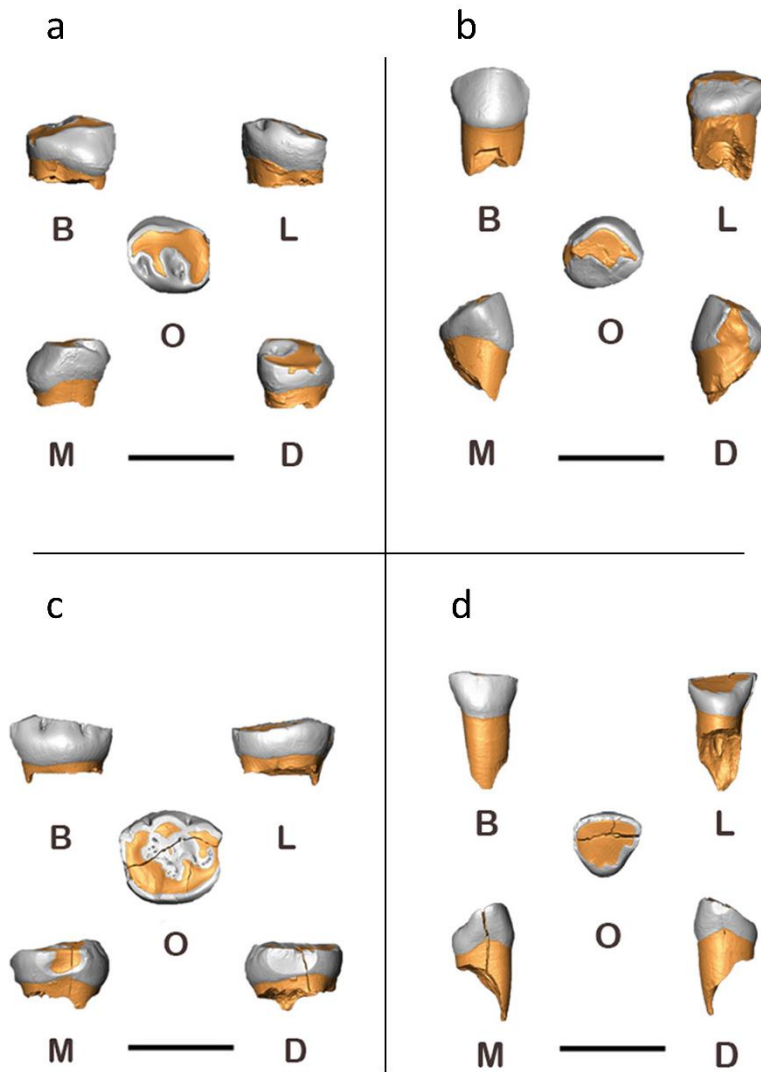
1124 3) Diagenesis is highly sample-specific even at the same site, illustrated here for Fumane
1125 cave, which makes a ‘one size fits all’ approach difficult to apply. While Fumane 2 is
1126 almost not affected by diagenesis that does also not affect Ba or Mg, the only slightly

1127 older Fumane 1 sample is more strongly overprinted, which manifests itself especially in
1128 Ba addition (>twofold increase) and Mg loss, while Sr is little affected.
1129 Overall, we note that diagenesis appears to affect the early formed enamel segments more
1130 than later mineralized areas. As the former are characterized by higher enamel extension
1131 rates, one conjecture is that this may have caused slightly greater amount of porosity that
1132 in turn makes such domains more susceptible for post-mortem chemical overprint. Thus,
1133 the initial portions of Nadale 1, Fumane 1 and Riparo Broion 1 crowns show enrichments
1134 in U, Al and Mn, with a concurrent decrease of Mg (Figure 3 and S9-S12). While Sr
1135 seems only partly affected by this overprint, Ba tends to precisely resemble the small-
1136 scale chemical fluctuations of the diagenetic proxies (clearly visible in Riparo Broion 1
1137 and Fumane 1), suggesting a lack of post-burial stability for the latter element.
1138 Taken together, we observe that the areas of interest (i.e. weaning onset) of our
1139 specimens are sufficiently free from diagenetic alterations to reliably deduce time-
1140 resolved dietary and mobility signals based on Sr/Ca and Sr isotopic ratios, respectively.
1141



1142

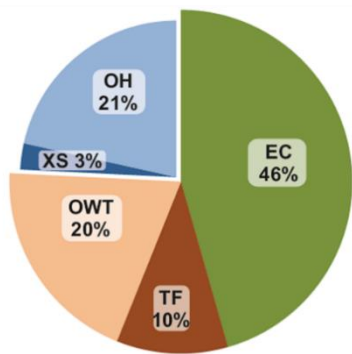
1143 **Figure S1. Micrographs acquired at 100x magnification of the four exfoliated**
1144 **deciduous fossil teeth.** (a) Nadale 1, Neanderthal, lower right deciduous first molar,
1145 lingual aspect, the section pass through the metaconid; (b) Fumane 1, Neanderthal, lower
1146 left deciduous second molar, buccal aspect, he section pass through the hypoconid; (c)
1147 Riparo Broion 1, Neanderthal, upper left deciduous canine, buccal aspect; (d) Fumane 2,
1148 UPMH, upper right lateral deciduous incisor, buccal aspect. Red lines highlight the
1149 position of the Neonatal line marking birth event; green lines highlight the laser ablation
1150 paths.



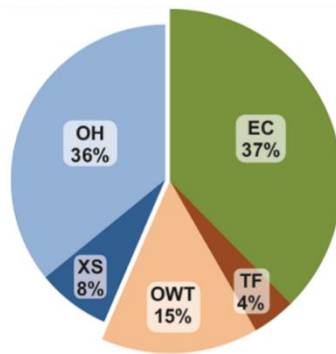
1151

1152 **Figure S2. Three-dimensional digital models of the four exfoliated deciduous fossil**
 1153 **teeth.** (a) Nadale 1 (lower right first deciduous molar); (b) Fumane 1 (lower left second
 1154 deciduous molar); (c) Riparo Broion 1 (upper right deciduous canine); (d) Fumane 2
 1155 (upper right lateral deciduous incisor). Scale bar 10 mm. B, buccal; D, distal; L, lingual;
 1156 M, mesial; O, occlusal

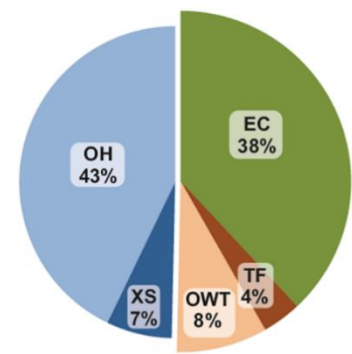
1157



Fimon pollen record
ca. 75-70 ka



Fimon pollen record
ca. 50-45 ka



Fimon pollen record
ca. 45-40 ka

1158

1159

1160

1161

1162

1163

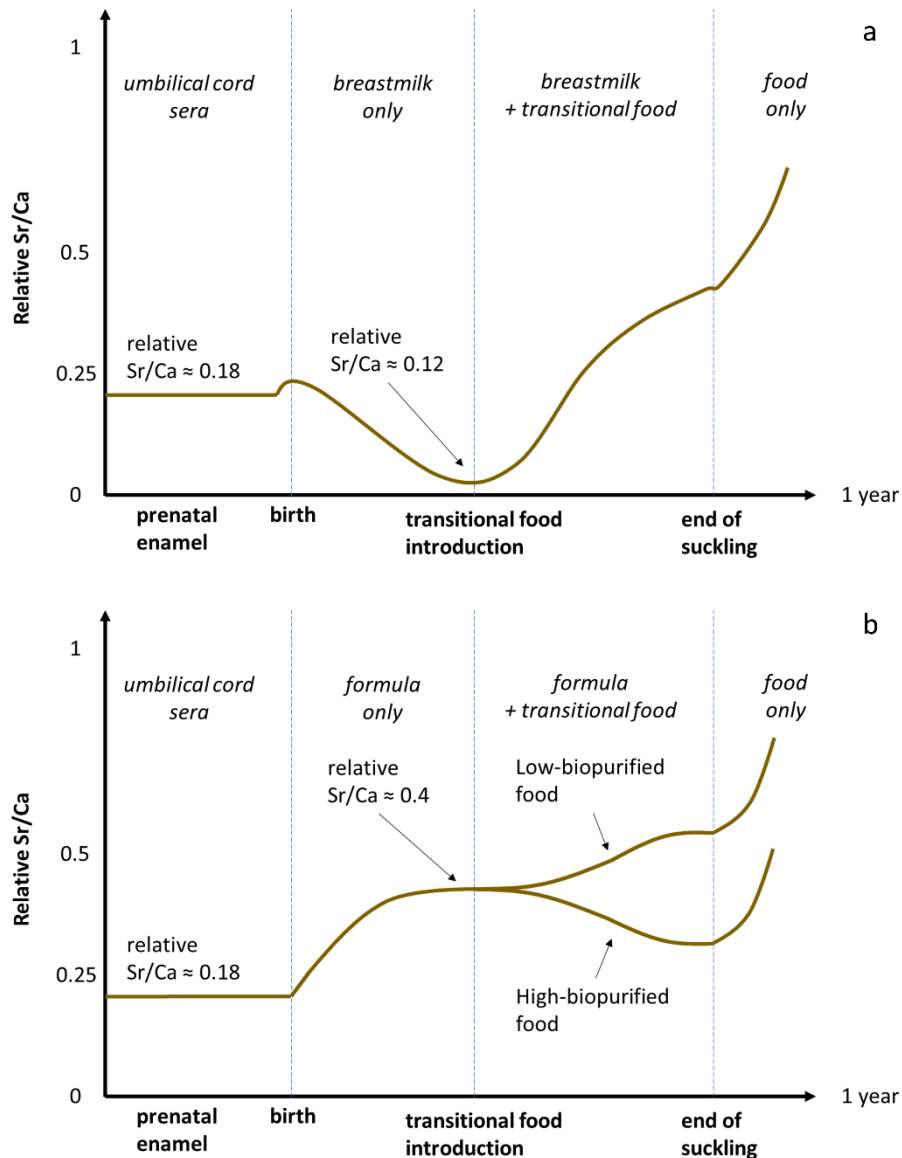
1164

1165

1166

1167

Figure S3. Pollen record summary of different vegetation types during selected time-frames. Pollen % are calculated based on the sum of terrestrial taxa and represent mean values over the selected time frame. Taxa are grouped according to their ecology and climatic preferences. Eurythermic conifers (EC): sum of *Pinus* and *Juniperus*; Temperate forest (TF): sum of deciduous *Quercus*, *Alnus glutinosa* type, *Fagus*, *Acer*, *Corylus*, *Carpinus*, *Fraxinus*, *Ulmus*, *Tilia* and *Salix*; Xerophytic steppe (XS): sum of *Artemisia* and Chenopodiaceae; other herbs (OH): sum of terrestrial herbs; other woody taxa (OWT) are also reported.

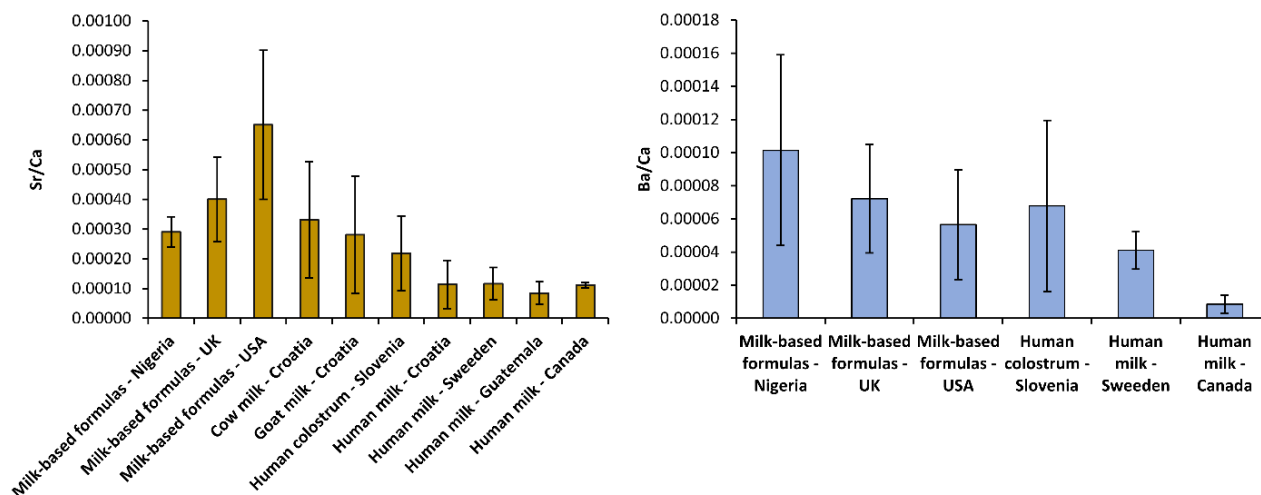


1168

1169 **Figure S4. Sr/Ca models for (a) breast-fed infants and (b) formula fed-infants.** These
 1170 models assume a mother diet equal to 1. In this model, GIT function is ignored since it
 1171 begins to significantly discriminate Sr over Ca at ~1 year of age in humans. A small peak
 1172 in Sr/Ca signal is visible across birth in breast-fed infants (a); this has been observed
 1173 empirically in our tooth samples and may relate to several factors, as e.g. high-metal
 1174 content of colostrum (57) or potential changes in perinatal physiology (56). The same
 1175 peak is probably masked in formula-fed infants (b) due to the rapid Sr/Ca increase.

1176

1177



1178

1179

1180 **Figure S5. Sr/Ca and Ba/Ca data of animal milks, human milks and formulas from**

1181 **literature.** Formulas are from Ikem et al. (72); cow and goat milks are from Bilandžić et

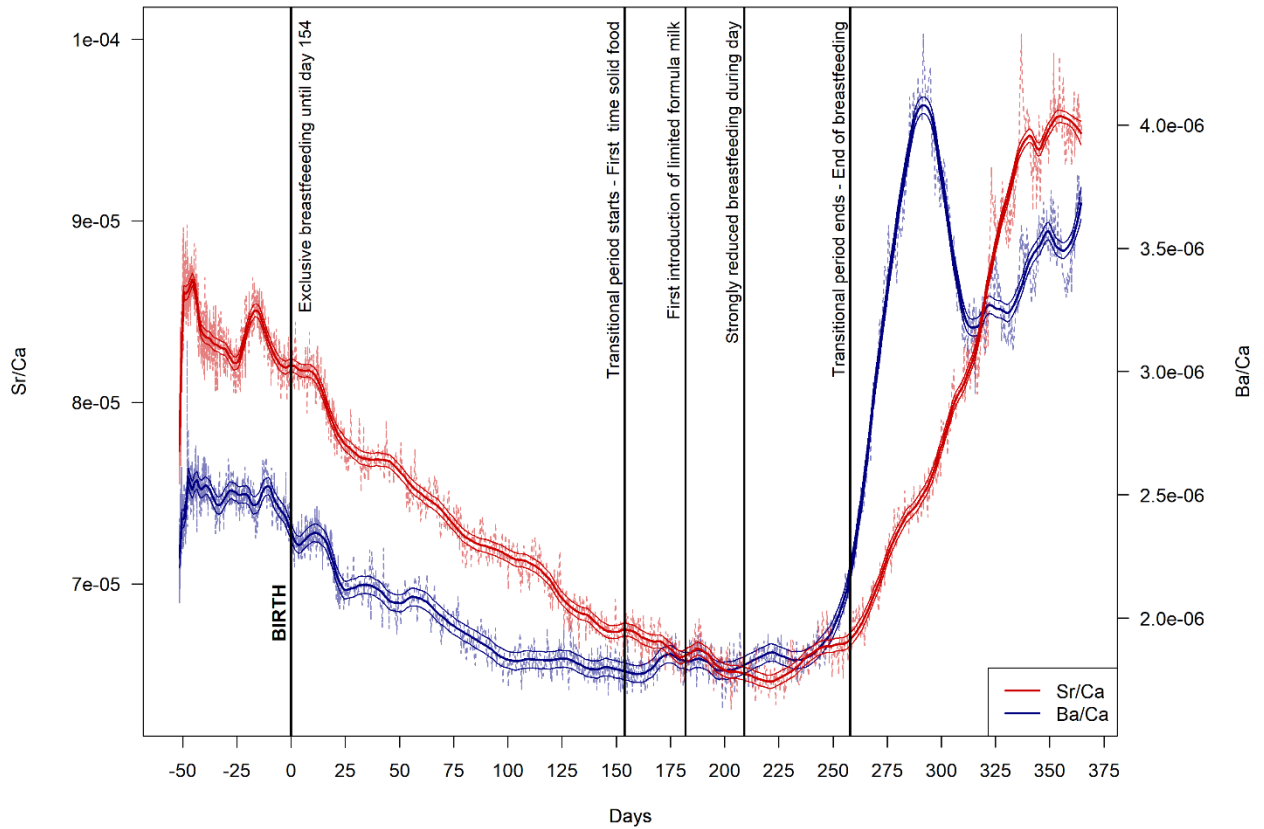
1182 al. (73); human colostrum is from Krachler et al. (55); human milks are from Bilandžić et

1183 al. (73), Björklund et al. (74), Li et al. (75) and Friel et al. (76). The geographical

1184 provenance of the samples is also reported. Error bars are standard deviations.

1185

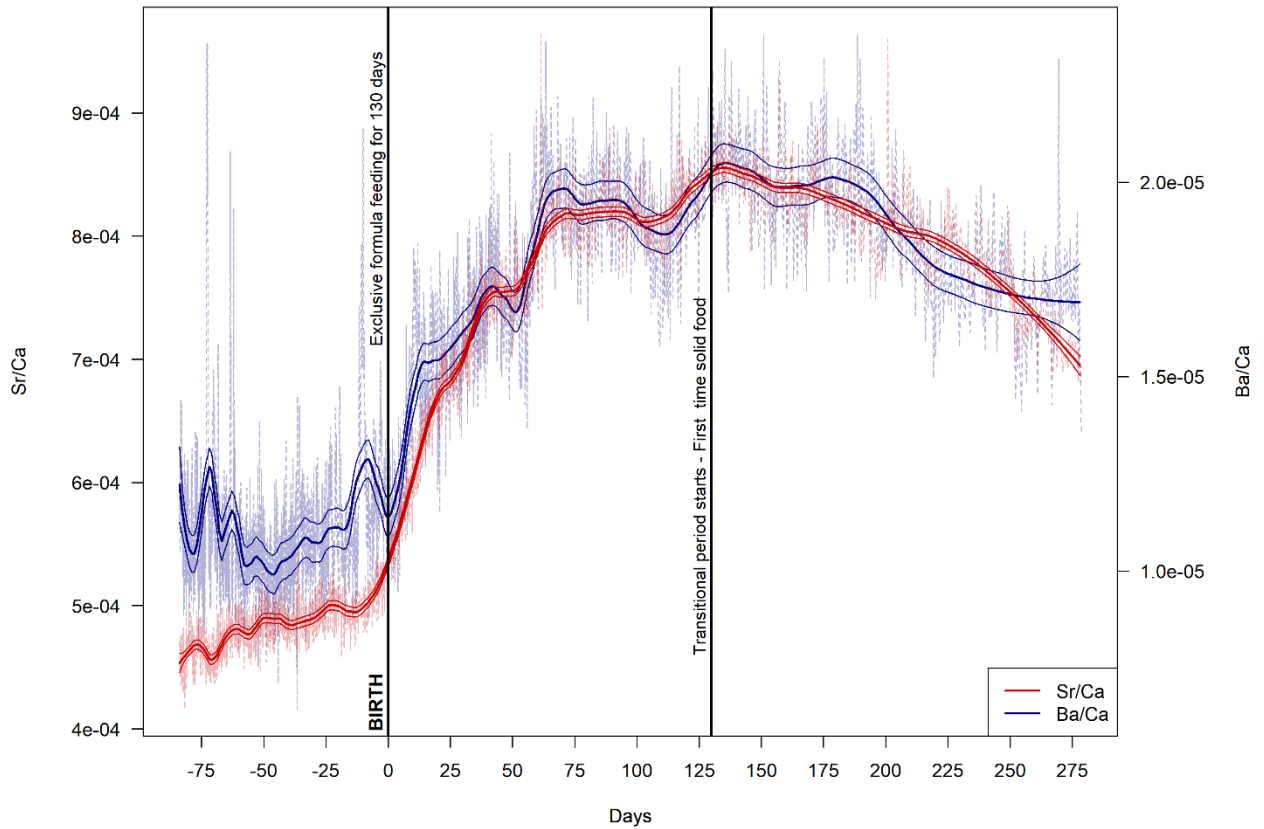
1186



1187

1188 **Figure S6. Time-resolved Sr/Ca and Ba/Ca profiles in modern reference deciduous**
 1189 **teeth of the exclusively breastfed individual MCS1.** Deciduous second molar dm2; The
 1190 elemental profiles were analyzed within enamel closest to the enamel-dentine-junction
 1191 (EDJ).

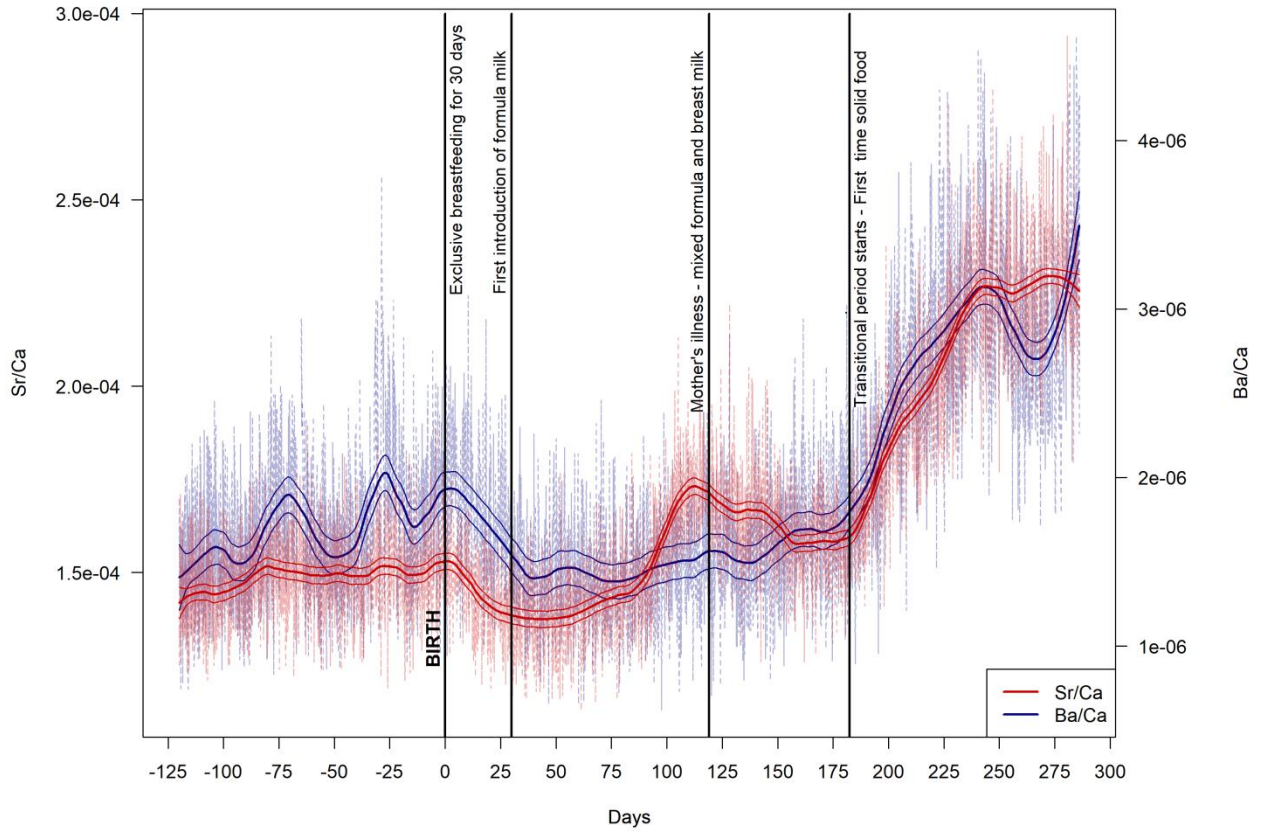
1192



1193

1194 **Figure S7. Time-resolved Sr/Ca and Ba/Ca profiles in modern reference deciduous**
 1195 **teeth of the exclusively formula-fed individual MCS2.** Deciduous canine dc. The
 1196 elemental profiles were analyzed within enamel closest to the enamel-dentine-junction
 1197 (EDJ).

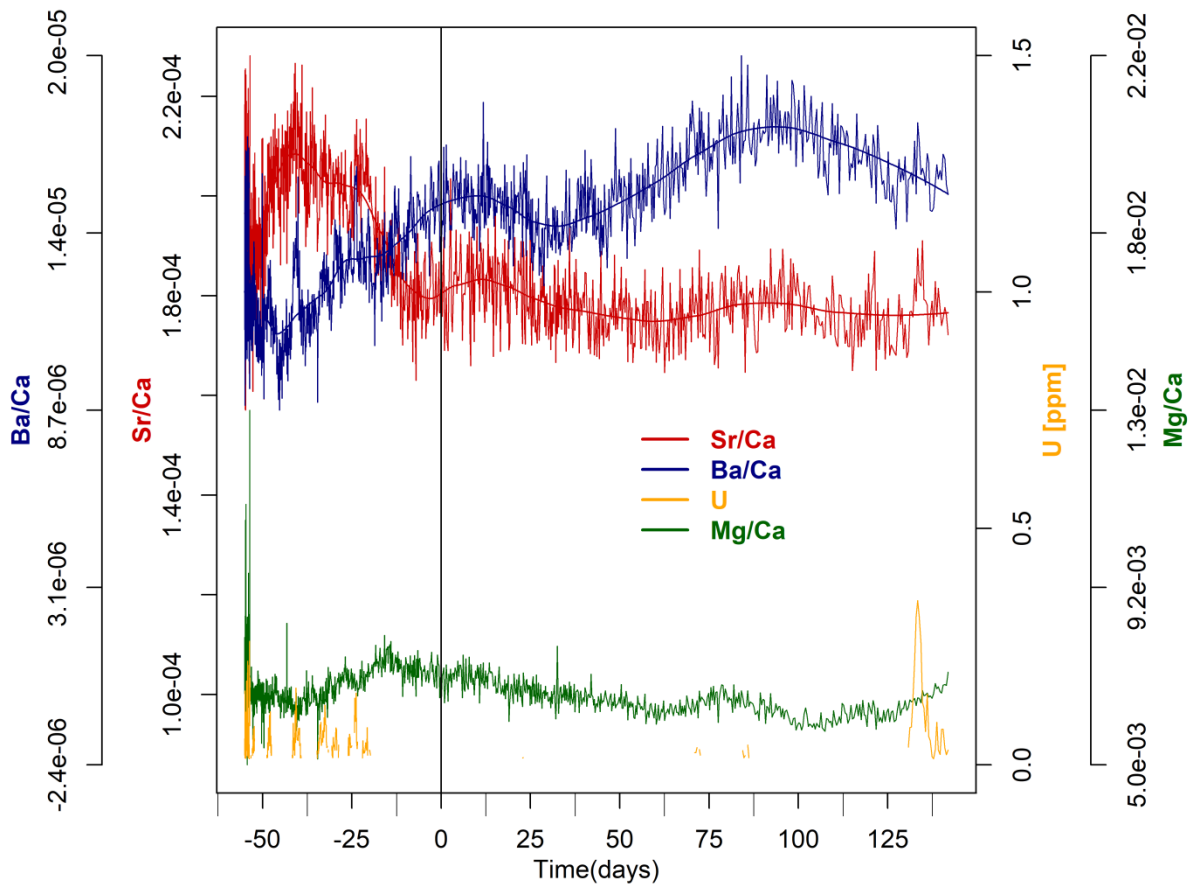
1198



1199

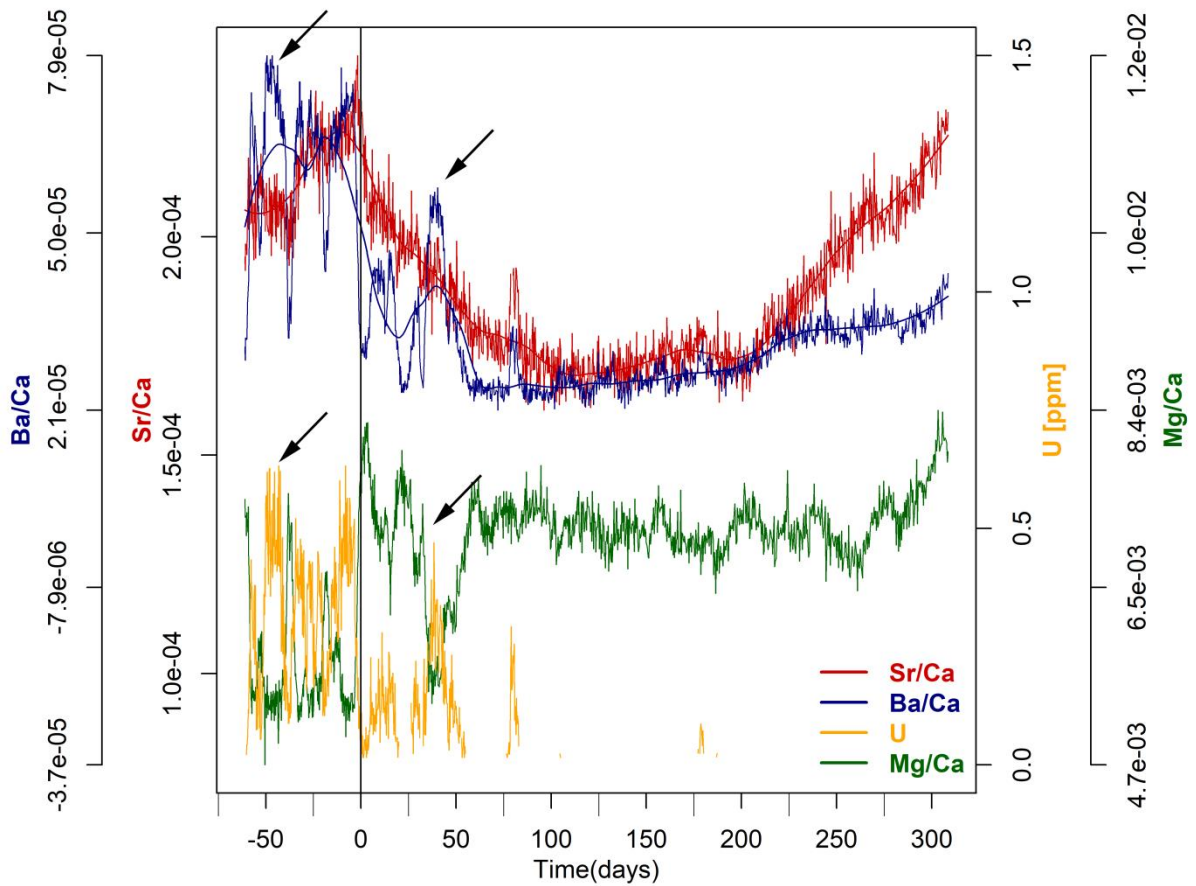
1200 **Figure S8. Time-resolved Sr/Ca and Ba/Ca profiles in modern reference deciduous**
 1201 **teeth of the mixed breast- formula-fed individual individual MCS3. deciduous canine**
 1202 **dc. The elemental profiles were analyzed within enamel closest to the enamel-dentine-**
 1203 **junction (EDJ).**

1204



1205
 1206
 1207
 1208
 1209
 1210

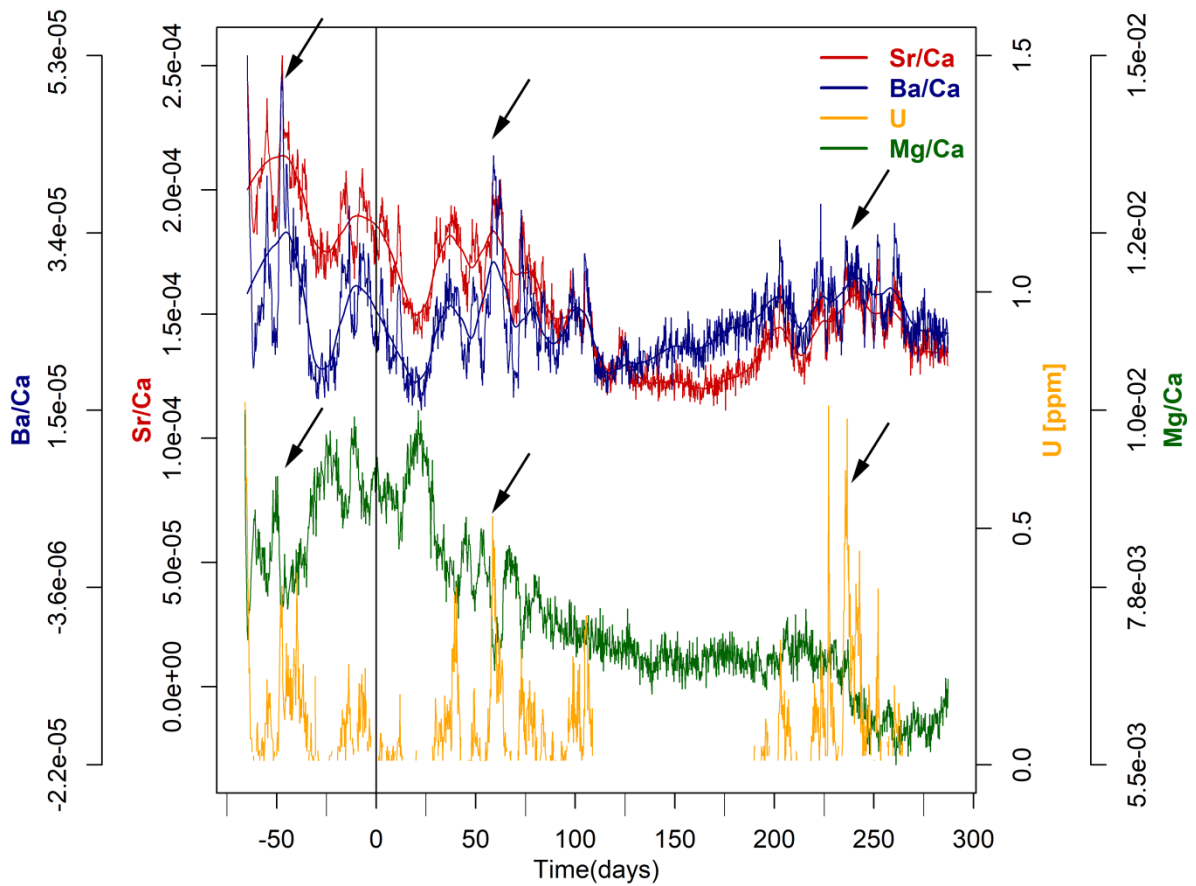
Figure S9. Time-resolved Sr/Ca, Ba/Ca, Mg/Ca and [U] profiles Nadale 1 deciduous teeth. The elemental profiles were analyzed within enamel closest to the enamel-dentine-junction (EDJ).



1211

1212 **Figure S10. Time-resolved Sr/Ca, Ba/Ca, Mg/Ca and [U] profiles Fumane 1**
 1213 **deciduous teeth.** The elemental profiles were analyzed within enamel closest to the
 1214 enamel-dentine-junction (EDJ); While Sr seems only partly affected by this overprint, Ba
 1215 tends to precisely resemble the small-scale chemical fluctuations of the diagenetic proxies
 1216 (i.e. U). The anticorrelation between U and Mg/Ca indicates a loss Mg during the post-
 1217 burial history, and the likely precipitation of low-Mg phases. Black arrows highlight the
 1218 worst diagenetically-affected domains of the enamel.

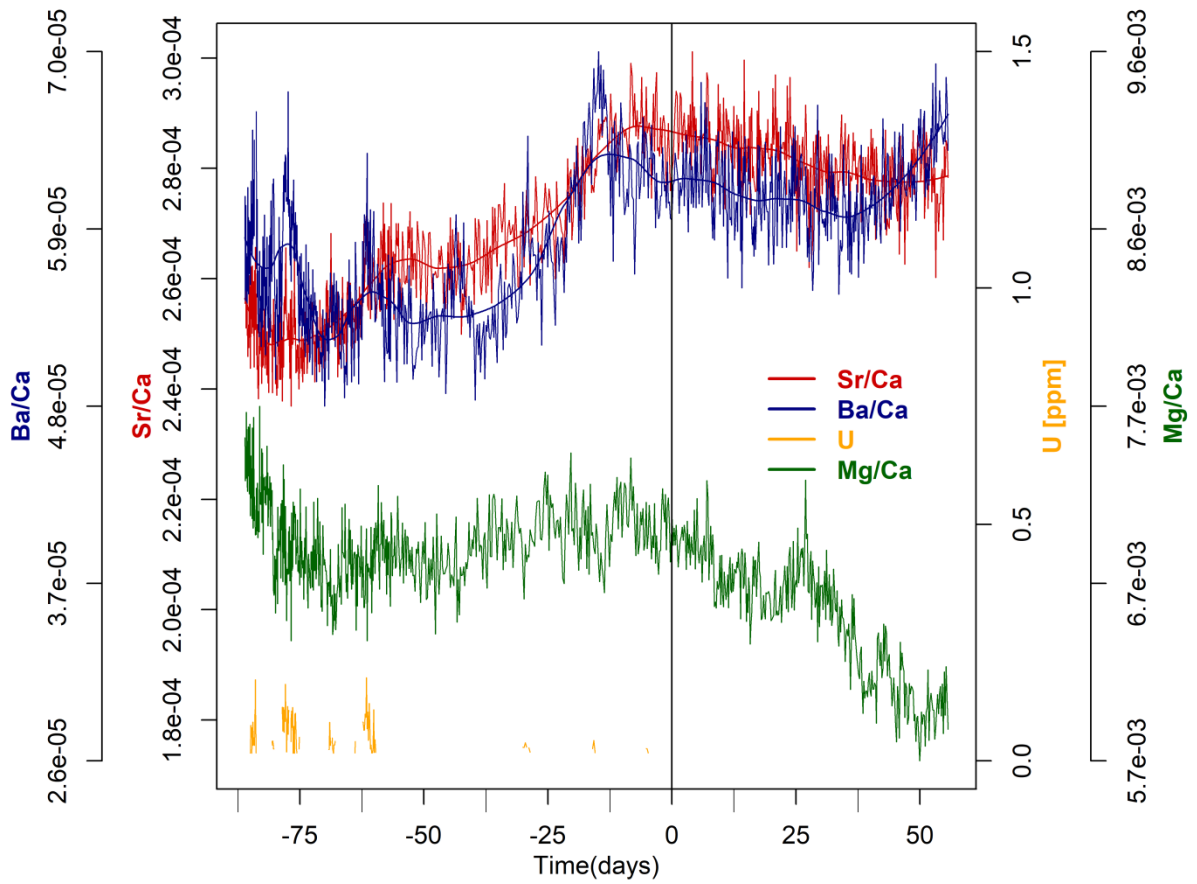
1219



1220

1221 **Figure S11. Time-resolved Sr/Ca, Ba/Ca, Mg/Ca and [U] profiles Riparo Broion 1**
 1222 **deciduous teeth.** The elemental profiles were analyzed within enamel closest to the
 1223 enamel-dentine-junction (EDJ); While Sr seems only partly affected by this overprint, Ba
 1224 tends to precisely resemble the small-scale chemical fluctuations of the diagenetic proxies
 1225 (i.e. U). The anticorrelation between U and Mg/Ca indicates a loss Mg during the post-
 1226 burial history, and the likely precipitation of low-Mg phases. Black arrows highlight the
 1227 worst diagenetically-affected domains of the enamel.

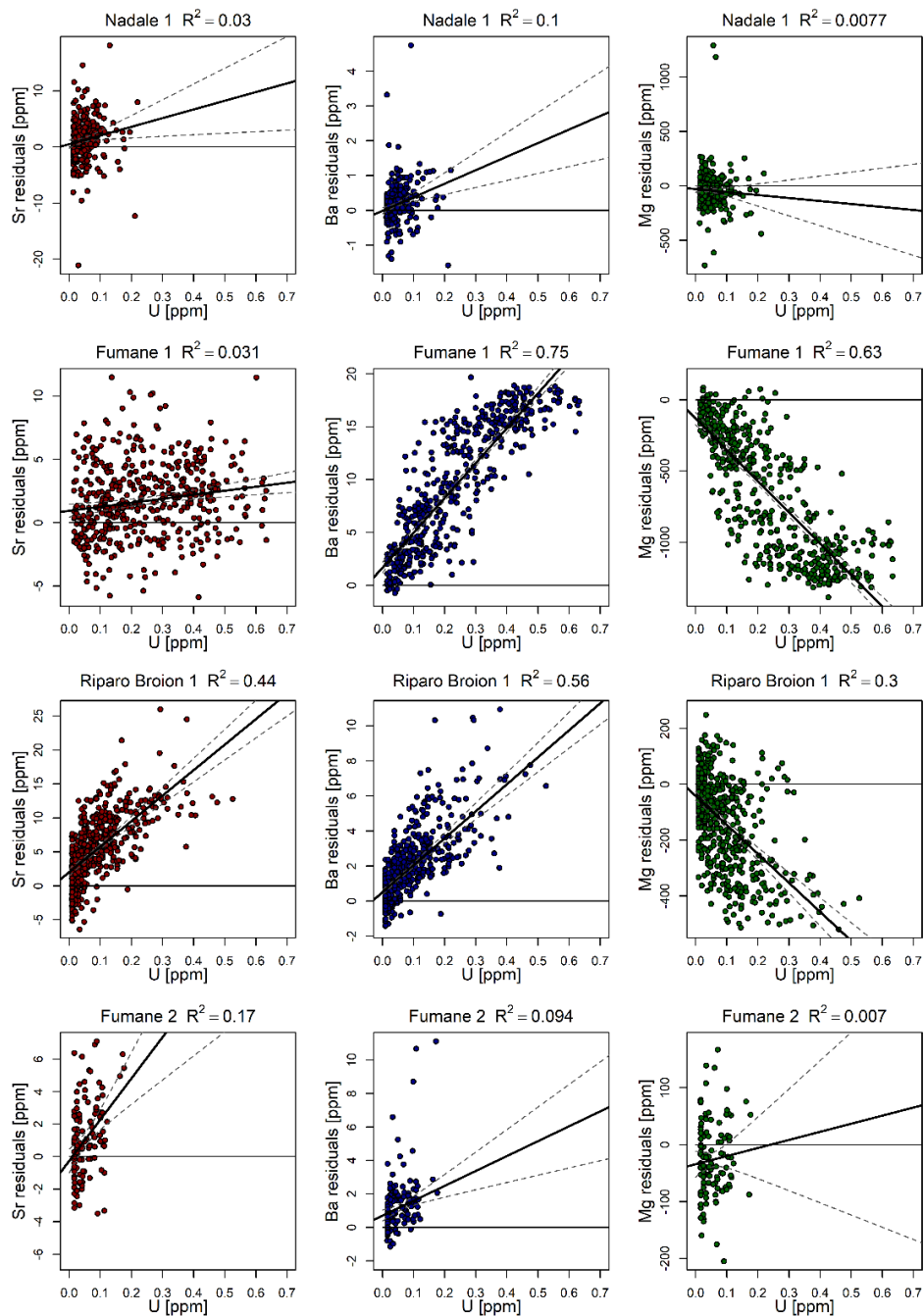
1228



1229

1230 **Figure S12. Time-resolved Sr/Ca, Ba/Ca, Mg/Ca and [U] profiles Fumane 2**
 1231 **deciduous tooth.** The elemental profiles were analyzed within enamel closest to the
 1232 enamel-dentine-junction (EDJ).

1233



1234
 1235
 1236
 1237
 1238
 1239
 1240
 1241

Fig. S13: Scatter plots of U vs. the residuals of Sr, Ba or Mg variation for the diagenetically most affected segments in Nadale 1 (start till -10days), Fumane 1 (start till 100 days), Riparo Broion 1(start till 125 days) and Fumane 2 (start till -50 days). Residuals were derived from the smoothed elemental profiles of Fig. 3e, calculated with a local polynomial regression fitting - LOWESS (77) - on the laser path portions with $U \leq LOD$. The residual Sr, Ba, Mg variability rather all data were used as we wanted as much as possible remove biological variation overprint any diagenesis signal.

Table S1: Sr isotopes of local rodent teeth by MC-ICPMS

| Site | Local geology | Rodent species | Sample type | $^{87}\text{Sr}/^{87}\text{Sr}$ | 2 S.E. |
|------------------|---|-----------------------------|---------------------------------------|---------------------------------|----------------|
| Nadale | Eocene limestone | <i>Microtinae</i> indet. | enamel | 0.70847 | 0.00001 |
| | | | enamel | 0.70843 | 0.00001 |
| | | | enamel | 0.70825 | 0.00003 |
| | | | enamel | 0.70864 | 0.00001 |
| | | | enamel | 0.70857 | 0.00001 |
| | | | mean (\pm 2 S.D.) | 0.70847 | 0.00030 |
| Riparo Broion | Eocene Oligocene limestone | <i>Microtinae</i> indet. | whole tooth | 0.70826 | 0.00001 |
| | | | whole tooth | 0.70820 | 0.00001 |
| | | | whole tooth | 0.70814 | 0.00001 |
| | | | whole tooth | 0.70827 | 0.00001 |
| | | | whole tooth | 0.70838 | 0.00001 |
| | | | mean (\pm 2 S.D.) | 0.70825 | 0.00018 |
| Fumane Cave | Jurassic-Cretaceous limestone and marl | <i>Microtinae</i> indet. | enamel | 0.70948 | 0.00001 |
| | | | enamel | 0.70937 | 0.00001 |
| | | | enamel | 0.70947 | 0.00001 |
| | | | enamel | 0.70940 | 0.00001 |
| | | | enamel | 0.70962 | 0.00001 |
| | | | enamel | 0.70958 | 0.00001 |
| | | | mean (\pm 2 S.D.) | 0.70948 | 0.00020 |

1242

1243

1244 **Table S2.** Discrimination factors of Sr over Ca within mother and infant bodies; fluxes
 1245 through different tissues are reported in brackets; a Sr/Ca relative to a mother diet equal
 1246 to 1 has been calculated for each end-member; the different enamel portions where a
 1247 specific signal is fixed are also reported.

| End-member (flux) | (Sr-over-Ca discrimination factor) | Relative Sr/Ca | Reference | Enamel |
|--|--|----------------|------------------------|-------------------------------|
| Diet | - | 1 | - | - |
| Mother sera (diet-blood) | 0.30 ± 0.08* | 0.3 | Balter, 2004 | - |
| Umbilical cord sera (mother sera - placenta) | 0.6 | 0.18 | ICRP, 2004 | prenatal |
| Breastmilk (mother sera - mammary gland) | 0.4 | 0.12 | ICRP, 2004 | postnatal, breast-fed infant |
| Animal milk | One trophic level lower than human breastmilk (Sr/Ca ~3.3-fold higher than human milk) | 0.40 | Balter, 2004; see text | postnatal, formula-fed infant |

*this value is relative to the difference between mammals' muscle (or bone) tissue and their diet, based on a large trophic chain study; for simplicity any eventual discrimination between blood and muscles (or bones) is ignored.

1248

1249

1250 **Table S3.** Ba, Sr, Ca, Ba/Ca and Sr/Ca values of umbilical cord sera, breast-fed infant
 1251 sera and formula-fed infant sera from (52, 55). Values are reported as mean \pm sd.

| Elemental contents and ratios | Maternal sera ^a | Umbilical cord sera ^b | Umbilical cord sera ^a | Breast-fed infant (ca. 3 months) sera ^b | Formula-fed infant (ca. 3 months) sera ^b | Colostrum ^a |
|--|----------------------------|----------------------------------|----------------------------------|--|---|------------------------|
| Ba ($\mu\text{g/L}$) | 6 \pm 7.8 | 0.8 \pm 0.8 | 1.5 \pm 1.7 | 1.9 \pm 0.4 | 3.8 \pm 1.4 | 10.6 \pm 8.7 |
| Sr ($\mu\text{g/L}$) | 22.3 \pm 8.9 | 20 \pm 9 | 19.6 \pm 7.2 | 12 \pm 3 | 40 \pm 25 | 37 \pm 18 |
| Ca (mg/L) | 92 \pm 16 | 95 \pm 13 | 104 \pm 16 | 112 \pm 4 | 116 \pm 8 | 210 \pm 60 |
| Ba/Ca*10³ | 0.082 \pm 0.093 | 0.010 \pm 0.009 | 0.017 \pm 0.018 | 0.017 \pm 0.004 | 0.034 \pm 0.014 | 0.068 \pm 0.052 |
| Sr/Ca*10³ | 0.267 \pm 0.135 | 0.228 \pm 0.121 | 0.204 \pm 0.096 | 0.108 \pm 0.031 | 0.361 \pm 0.238 | 0.218 \pm 0.126 |

^aKrachler et al. (1999, *European Journal of Clinical Nutrition*); ^bKrachler et al. (1999, *Biological Trace Element Research*)

1252

1253

1254 **Legends for Datasets**

1255

1256 **Dataset S1.** $^{87}\text{Sr}/^{86}\text{Sr}$, $^{84}\text{Sr}/^{86}\text{Sr}$ and $^{85}\text{Rb}/^{86}\text{Sr}$ data of Middle-Upper Paleolithic deciduous
1257 teeth (baseline, interference, mass-bias/elemental-fractionation-corrected (see text); very
1258 minor offset of $^{84}\text{Sr}/^{86}\text{Sr}$ from 0.0565 is due to residual variability of ^{84}Kr -backgrounds
1259 for protracted profile analyses).

1260

1261 **Dataset S2.** Sr/Ca and Ba/Ca data of modern reference deciduous teeth.

1262

1263 **Dataset S3.** Sr/Ca, Ba/Ca, Mg/Ca and [U] data of Middle-Upper Paleolithic deciduous
1264 teeth (LOD indicates that [U]<limit of detection).

1265

1266 **SI References**

1267

- 1268 1. Benazzi S, *et al.* (2014) Middle Paleolithic and Uluzzian human remains from
1269 Fumane Cave, Italy. *Journal of Human Evolution* 70:61-68.
- 1270 2. Arnaud J, *et al.* (2017) A Neanderthal deciduous human molar with incipient
1271 carious infection from the Middle Palaeolithic De Nadale cave, Italy. *American*
1272 *journal of physical anthropology* 162(2):370-376.
- 1273 3. Benazzi S, *et al.* (2015) The makers of the Protoaurignacian and implications for
1274 Neandertal extinction. *Science* 348(6236):793-796.
- 1275 4. AlQahtani SJ, Hector M, & Liversidge H (2010) Brief communication: the
1276 London atlas of human tooth development and eruption. *American Journal of*
1277 *Physical Anthropology* 142(3):481-490.
- 1278 5. Jequier CA, *et al.* (2015) The De Nadale Cave, a single layered Quina Mousterian
1279 site in the North of Italy.
- 1280 6. Livraghi A, Fanfarillo G, Dal Colle M, Romandini M, & Peresani M (2019)
1281 Neanderthal ecology and the exploitation of cervids and bovids at the onset of
1282 MIS4: A study on De Nadale cave, Italy. *Quaternary International*.
- 1283 7. Terlato G, Livraghi A, Romandini M, & Peresani M (2019) Large bovids on the
1284 Neanderthal menu: Exploitation of *Bison priscus* and *Bos primigenius* in
1285 northeastern Italy. *Journal of Archaeological Science: Reports* 25:129-143.
- 1286 8. López-García JM, Livraghi A, Romandini M, & Peresani M (2018) The De
1287 Nadale Cave (Zovencedo, Berici Hills, northeastern Italy): A small-mammal
1288 fauna from near the onset of Marine Isotope Stage 4 and its palaeoclimatic
1289 implications. *Palaeogeography, Palaeoclimatology, Palaeoecology* 506:196-201.
- 1290 9. Martellotta E, Livraghi A, & Peresani M (in press) Bone retouchers from the
1291 Mousterian Quina site of De Nadale Cave (Berici Hills, north-eastern Italy).
1292 *Comptes Rendu Palevol*.
- 1293 10. Broglio A, Cilli C, Giacobini G, & Gurioli F (2006) Osso, palco, dente e
1294 conchiglia: i supporti in materia dura animale dei manufatti dei primi uomini
1295 moderni a Fumane (Verona). *XXXIX Riunione Scientifica Istituto Italiano*
1296 *Preistoria e Protostoria "Materie prime e scambi nella preistoria italiana"*,
1297 (Istituto Italiano Preistoria e Protostoria), pp 815-827.
- 1298 11. Peresani M (2012) Fifty thousand years of flint knapping and tool shaping across
1299 the Mousterian and Uluzzian sequence of Fumane cave. *Quaternary International*
1300 247:125-150.
- 1301 12. Peresani M, Cristiani E, & Romandini M (2016) The Uluzzian technology of
1302 Grotta di Fumane and its implication for reconstructing cultural dynamics in the
1303 Middle–Upper Palaeolithic transition of Western Eurasia. *Journal of human*
1304 *evolution* 91:36-56.
- 1305 13. Peresani M, *et al.* (2008) Age of the final Middle Palaeolithic and Uluzzian levels
1306 at Fumane Cave, Northern Italy, using ¹⁴C, ESR, ²³⁴U/²³⁰Th and
1307 thermoluminescence methods. *J. Archaeol. Sci.* 35(11):2986-2996.
- 1308 14. Higham T, *et al.* (2009) Problems with radiocarbon dating the Middle to Upper
1309 Palaeolithic transition in Italy. *Quaternary Science Reviews* 28(13-14):1257-1267.

- 1310 15. López-García JM, dalla Valle C, Cremaschi M, & Peresani M (2015)
 1311 Reconstruction of the Neanderthal and Modern Human landscape and climate
 1312 from the Fumane cave sequence (Verona, Italy) using small-mammal
 1313 assemblages. *Quaternary Science Reviews* 128:1-13.
- 1314 16. Fiore I, Gala M, & Tagliacozzo A (2004) Ecology and subsistence strategies in
 1315 the Eastern Italian Alps during the Middle Palaeolithic. *International Journal of*
 1316 *Osteoarchaeology* 14(3-4):273-286.
- 1317 17. Falcucci A, Conard NJ, & Peresani M (2017) A critical assessment of the
 1318 Protoaurignacian lithic technology at Fumane Cave and its implications for the
 1319 definition of the earliest Aurignacian. *PloS one* 12(12).
- 1320 18. Falcucci A, Peresani M, Roussel M, Normand C, & Soressi M (2018) What's the
 1321 point? Retouched bladelet variability in the Protoaurignacian. Results from
 1322 Fumane, Isturitz, and Les Cottés. *Archaeological and Anthropological Sciences*
 1323 10(3):539-554.
- 1324 19. Peresani M, *et al.* (2019) Marine and freshwater shell exploitation in the Early
 1325 Upper Palaeolithic. Re-examination of the assemblages from Fumane Cave (NE
 1326 Italy).
- 1327 20. Cavallo G, *et al.* (2018) Heat Treatment of Mineral Pigment During the Upper
 1328 Palaeolithic in North-East Italy. *Archaeometry* 60(5):1045-1061.
- 1329 21. Peretto C, Biagi P, Boschian G, & Broglio A (2004) Living-floors and structures
 1330 from the Lower Paleolithic to the Bronze Age in Italy. *Collegium antropologicum*
 1331 28(1):63-88.
- 1332 22. Broglio A, *et al.* (2003) L'Aurignacien dans le territoire préalpin: la Grotte de
 1333 Fumane. *XIV UISPP Congress*, (British Archaeological Reports), pp 93-104.
- 1334 23. Cassoli P & Tagliacozzo A (1994) Considerazioni paleontologiche,
 1335 paleoecologiche e archeozoologiche sui macromammiferi e gli uccelli dei livelli
 1336 del Pleistocene superiore del Riparo di Fumane (VR) scavi 1988-91. *Boll. Mus.*
 1337 *Civ. Stor. Nat. Verona* 18:349-445.
- 1338 24. Broglio A, Bertola S, De Stefani M, & Gurioli F (2009) The shouldered points of
 1339 the Early Epigravettian of the Berici Hills (Venetian Region-North Italy).
 1340 Materials, Blanks, Typology, Exploitation.
- 1341 25. Sauro U (2002) The Monti Berici: a peculiar type of karst in the Southern Alps.
 1342 *Acta Carsologica* 31(3):99-114.
- 1343 26. Dal Lago A & Mietto P (2003) Grotte dei Berici. *Aspetti fisici e naturalistici.*
 1344 *Museo Naturalistico Archeologico, Vicenza.*
- 1345 27. Peresani M & Porraz G (2004) Ré-interprétation et mise en valeur des niveaux
 1346 moustériens de la Grotte du Broion (Monti Berici, Vénétie). Etude techno-
 1347 économique des industries lithiques.
- 1348 28. Romandini M, Bertola S, & Nannini N (2015) Nuovi dati sul Paleolitico dei Colli
 1349 Berici: risultati preliminari dello studio archeozoologico e delle materie prime
 1350 litiche della Grotta del Buso Doppio del Broion (Lumignano, Longare, Vicenza).
 1351 *Nuovi dati sul Paleolitico dei Colli Berici: risultati preliminari dello studio*
 1352 *archeozoologico e delle materie prime litiche della Grotta del Buso Doppio del*
 1353 *Broion (Lumignano, Longare, Vicenza):53-59.*

- 1354 29. De Stefani M, Gurioli F, & Ziggiotti S (2005) Il Paleolitico superiore del Riparo
1355 del Broion nei Colli Berici (Vicenza). *Il Paleolitico superiore del Riparo del*
1356 *Broion nei Colli Berici (Vicenza)*:93-108.
- 1357 30. Peresani M, Bertola S, Delpiano D, Benazzi S, & Romandini M (2019) The
1358 Uluzzian in the north of Italy: insights around the new evidence at Riparo Broion.
1359 *Archaeological and Anthropological Sciences* 11(7):3503-3536.
- 1360 31. Romandini M, *et al.* (in review) A late Neanderthal tooth from northeastern Italy.
1361 *Journal of Human Evolution*.
- 1362 32. Vescovi E, *et al.* (2007) Interactions between climate and vegetation on the
1363 southern side of the Alps and adjacent areas during the Late-glacial period as
1364 recorded by lake and mire sediment archives. *Quaternary Science Reviews*
1365 26:1650-1669.
- 1366 33. Badino F, *et al.* (2019) An overview of Alpine and Mediterranean
1367 palaeogeography, terrestrial ecosystems and climate history during MIS 3 with
1368 focus on the Middle to Upper Palaeolithic transition. *Quaternary International*.
- 1369 34. Pini R, Ravazzi C, & Reimer P (2010) The vegetation and climate history of the
1370 last glacial cycle in a new pollen record from Lake Fimon (southern Alpine
1371 foreland, N-Italy). *Quaternary Science Reviews* 29(23-24):3115-3137.
- 1372 35. Shannon R (1976) Revised effective ionic radii and systematic studies of
1373 interatomic distances in halides and chalcogenides. *Acta crystallographica section*
1374 *A: crystal physics, diffraction, theoretical and general crystallography* 32(5):751-
1375 767.
- 1376 36. Burton JH, Price TD, & Middleton WD (1999) Correlation of bone Ba/Ca and
1377 Sr/Ca due to biological purification of calcium. *J. Archaeol. Sci.* 26(6):609-616.
- 1378 37. Elias RW, Hirao Y, & Patterson CC (1982) The Circumvention of the Natural
1379 Biopurification of Calcium along Nutrient Pathways by Atmospheric Inputs of
1380 Industrial Lead. *Geochimica et Cosmochimica Acta* 46(12):2561-2580.
- 1381 38. Balter V (2004) Allometric constraints on Sr/Ca and Ba/Ca partitioning in
1382 terrestrial mammalian trophic chains. *Oecologia* 139(1):83-88.
- 1383 39. Dahl S, *et al.* (2001) Incorporation and distribution of strontium in bone. *Bone*
1384 28(4):446-453.
- 1385 40. Kshirsagar S, Lloyd E, & Vaughan J (1966) Discrimination between strontium
1386 and calcium in bone and the transfer from blood to bone in the rabbit. *The British*
1387 *Journal of Radiology* 39(458):131-140.
- 1388 41. Burton JH & Wright LE (1995) Nonlinearity in the relationship between bone
1389 Sr/Ca and diet: paleodietary implications. *American journal of physical*
1390 *anthropology* 96(3):273-282.
- 1391 42. Price TD, Swick RW, & Chase EP (1986) Bone chemistry and prehistoric diet:
1392 strontium studies of laboratory rats. *American Journal of Physical Anthropology*
1393 70(3):365-375.
- 1394 43. Gilbert C, Sealy J, & Sillen A (1994) An investigation of barium, calcium and
1395 strontium as palaeodietary indicators in the Southwestern Cape, South Africa. *J.*
1396 *Archaeol. Sci.* 21(2):173-184.
- 1397 44. Rivera J & Harley JH (1965) The HASL Bone Program, 1961-1964. (Health and
1398 Safety Lab., New York Operations Office (AEC), NY).

- 1399 45. Sillen A & Smith P (1984) Weaning patterns are reflected in strontium-calcium
1400 ratios of juvenile skeletons. *J. Archaeol. Sci.* 11(3):237-245.
- 1401 46. Lough S, Rivera J, & Comar C (1963) Retention of strontium, calcium, and
1402 phosphorus in human infants. *Proceedings of the Society for Experimental*
1403 *Biology and Medicine* 112(3):631-636.
- 1404 47. Rossipal E, Krachler M, Li F, & Micetic-Turk D (2000) Investigation of the
1405 transport of trace elements across barriers in humans: studies of placental and
1406 mammary transfer. *Acta Paediatrica* 89(10):1190-1195.
- 1407 48. ICRP (2004) Doses to infants from ingestion of radionuclides in mother's milk.
1408 *ICRP Publication 95. Ann. ICRP* 34(3-4).
- 1409 49. Humphrey LT, Dean MC, Jeffries TE, & Penn M (2008) Unlocking evidence of
1410 early diet from tooth enamel. *Proceedings of the National Academy of Sciences of*
1411 *the United States of America* 105(19):6834-6839.
- 1412 50. Müller W, *et al.* (2019) Enamel mineralization and compositional time-resolution
1413 in human teeth evaluated via histologically-defined LA-ICPMS profiles.
1414 *Geochimica et Cosmochimica Acta* 255:105-126.
- 1415 51. Humphrey LT, Dirks W, Dean MC, & Jeffries TE (2008) Tracking dietary
1416 transitions in weanling baboons (*Papio hamadryas anubis*) using
1417 strontium/calcium ratios in enamel. *Folia Primatologica* 79(4):197-212.
- 1418 52. Krachler M, Rossipal E, & Micetic-Turk D (1999) Concentrations of trace
1419 elements in sera of newborns, young infants, and adults. *Biological trace element*
1420 *research* 68(2):121.
- 1421 53. Peek S & Clementz MT (2012) Sr/Ca and Ba/Ca variations in environmental and
1422 biological sources: a survey of marine and terrestrial systems. *Geochimica et*
1423 *Cosmochimica Acta* 95:36-52.
- 1424 54. Austin C, *et al.* (2013) Barium distributions in teeth reveal early-life dietary
1425 transitions in primates. *Nature* 498(7453):216-219.
- 1426 55. Krachler M, Rossipal E, & Micetic-Turk D (1999) Trace element transfer from
1427 the mother to the newborn—investigations on triplets of colostrum, maternal and
1428 umbilical cord sera. *European journal of clinical nutrition* 53(6):486-494.
- 1429 56. Dean MC, Spiers KM, Garrevoet J, & Le Cabec A (2019) Synchrotron X-ray
1430 fluorescence mapping of Ca, Sr and Zn at the neonatal line in human deciduous
1431 teeth reflects changing perinatal physiology. *Archives of oral biology* 104:90-102.
- 1432 57. Matos C, Moutinho C, Almeida C, Guerra A, & Balcão V (2014) Trace element
1433 compositional changes in human milk during the first four months of lactation.
1434 *International journal of food sciences and nutrition* 65(5):547-551.
- 1435 58. Metcalfe JZ, Longstaffe FJ, & Zazula GD (2010) Nursing, weaning, and tooth
1436 development in woolly mammoths from Old Crow, Yukon, Canada: implications
1437 for Pleistocene extinctions. *Palaeogeography, Palaeoclimatology, Palaeoecology*
1438 298(3-4):257-270.
- 1439 59. Tacail T, Kovačiková L, Brůžek J, & Balter V (2017) Spatial distribution of trace
1440 element Ca-normalized ratios in primary and permanent human tooth enamel.
1441 *Science of the Total Environment* 603:308-318.

- 1442 60. Taylor D, Bligh P, & Duggan MH (1962) The absorption of calcium, strontium,
1443 barium and radium from the gastrointestinal tract of the rat. *Biochemical journal*
1444 83(1):25.
- 1445 61. Gillespie B, d'Arcy H, Schwartz K, Bobo JK, & Foxman B (2006) Recall of age
1446 of weaning and other breastfeeding variables. *International Breastfeeding Journal*
1447 1:4-4.
- 1448 62. Hoppe KA, Koch PL, & Furutani TT (2003) Assessing the preservation of
1449 biogenic strontium in fossil bones and tooth enamel. *International Journal of*
1450 *Osteoarchaeology* 13(1-2):20-28.
- 1451 63. Hinz EA & Kohn MJ (2010) The effect of tissue structure and soil chemistry on
1452 trace element uptake in fossils. *Geochimica et Cosmochimica Acta* 74(11):3213-
1453 3231.
- 1454 64. Radosevich SC (1993) The Six Deadly Sins of Trace Element Analysis: A Case of
1455 Wishful Thinking in Science. *Investigations of Ancient Human Tissue: Chemical*
1456 *Analyses in Anthropology*, ed Sandford MK (Gordon and Breach), pp 269-332.
- 1457 65. Kohn MJ & Moses RJ (2013) Trace element diffusivities in bone rule out simple
1458 diffusive uptake during fossilization but explain in vivo uptake and release.
1459 *Proceedings of the National Academy of Sciences* 110(2):419-424.
- 1460 66. Reynard B & Balter V (2014) Trace elements and their isotopes in bones and
1461 teeth: diet, environments, diagenesis, and dating of archeological and
1462 paleontological samples. *Palaeogeography, Palaeoclimatology, Palaeoecology*
1463 416:4-16.
- 1464 67. Millard AR & Hedges REM (1996) A diffusion-adsorption model of uranium
1465 uptake by archaeological bone. *Geochim. Cosmochim. Acta* 60(12):2139-2152.
- 1466 68. Krestou A, Xenidis A, & Papias D (2004) Mechanism of aqueous uranium (VI)
1467 uptake by hydroxyapatite. *Minerals Engineering* 17(3):373-381.
- 1468 69. Grün R, Aubert M, Joannes-Boyau R, & Moncel M-H (2008) High resolution
1469 analysis of uranium and thorium concentration as well as U-series isotope
1470 distributions in a Neanderthal tooth from Payre (Ardèche, France) using laser
1471 ablation ICP-MS. *Geochim. Cosmochim. Acta* 72(21):5278-5290.
- 1472 70. Trueman CN & Tuross N (2002) Trace elements in recent and fossil bone apatite.
1473 *Reviews in mineralogy and geochemistry* 48(1):489-521.
- 1474 71. Turner-Walker G & Peacock EE (2008) Preliminary results of bone diagenesis in
1475 Scandinavian bogs. *Palaeogeography, Palaeoclimatology, Palaeoecology* 266(3-
1476 4):151-159.
- 1477 72. Ikem A, Nwankwoala A, Oduyungbo S, Nyavor K, & Egiebor N (2002) Levels
1478 of 26 elements in infant formula from USA, UK, and Nigeria by microwave
1479 digestion and ICP-OES. *Food Chemistry* 77(4):439-447.
- 1480 73. Bilandžić N, *et al.* (2011) Trace element levels in raw milk from northern and
1481 southern regions of Croatia. *Food chemistry* 127(1):63-66.
- 1482 74. Björklund KL, *et al.* (2012) Metals and trace element concentrations in breast
1483 milk of first time healthy mothers: a biological monitoring study. *Environmental*
1484 *Health* 11(1):92.

- 1485 75. Li C, Solomons NW, Scott ME, & Koski KG (2016) Minerals and trace elements
1486 in human breast milk are associated with Guatemalan infant anthropometric
1487 outcomes within the first 6 months. *The Journal of nutrition* 146(10):2067-2074.
- 1488 76. Friel JK, *et al.* (1999) Elemental composition of human milk from mothers of
1489 premature and full-term infants during the first 3 months of lactation. *Biological*
1490 *trace element research* 67(3):225-247.
- 1491 77. Cleveland W, Grosse E, & Shyu W (1992) Local regression models. In 'Statistical Models
1492 in S'. (Eds JM Chambers, TJ Hastie) pp. 309–376. (Chapman & Hall: New York).1.
- 1493 Sellen DW (2007) Evolution of infant and young child feeding: implications for
1494 contemporary public health. *Annu. Rev. Nutr.* 27:123-148.
- 1495